NICKEL IN STAINLESS STEELS

C.P. Cutler[1], G.E. Coates[1], D.C. Jenkinson[2]

[1]Nickel Institute,United Kingdom, [2]Consultant to Nickel Institute, United Kingdom

Abstract

Nickel is widely used as an alloying element in many stainless steels but the recent increased raw material cost has encouraged users to look at lower nickel or nickel-free alloys. However, initial cost is not the only issue – service performance over the life of a component is much more significant to the user. This paper looks at the rôle of nickel and how it contributes to fabricability, toughness, corrosion resistance and high temperature strength.

The process of material selection to achieve the desired combination of economic and other performance characteristics over the full life cycle of a product is examined. To have maximum confidence in the outcome of the selection, it is necessary to have both good data on the alloys and also a history of service performance. However, the final material choice is a balance of many factors including availablity, fabricability and environmental benefits.

Case studies illustrate potential material choices and demonstrate how nickel continues to be an important alloying element, giving cost-effective service.

Metallurgy

Chromium is the key alloying element which makes stainless steels “stainless”. More than 10.5% needs to be added to steel to allow the protective oxide film to form which provides the corrosion resistance and bright, silvery appearance. In general, the more chromium which is added, the greater the corrosion resistance. That discovery was made about a century ago yet even some of those early stainless steels also contained nickel. Today about two thirds of the tonnage of stainless steel produced each year contains nickel, even though nickel is an expensive alloying addition. What is the rôle of nickel and why is it used so extensively?

Metals with an austenitic (face centred cubic) crystal structure are particularly tough and ductile. Aluminium, copper and nickel itself are good examples. Nickel is an austenite forming alloying addition which can produce stainless steels having an austenitic structure, stable at room temperature, see Figure 1.

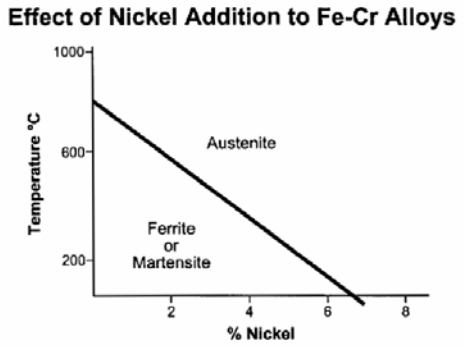

Figure 1. The effect of nickel.[1]

Austenitic stainless steels have a particularly attractive combination of properties. That is the primary reason for adding nickel and gives rise to the most common grade of stainless steel in use today, Type 304, often referred to as "18/8" since it has the approximate composition 18 % chromium and 8 % nickel.

There are other alloying elements which are austenite formers, most notably carbon, nitrogen, manganese and copper. The relative effectiveness of them as austenite formers can be seen in the expression:

$$\text{Nickel equivalent} = Ni\% + 30C\% + 30N\% + 0.5Mn\% + 0.3Cu\% \quad \text{(by weight)}$$

Manganese was first used as an addition to stainless steel in the 1930's. The 200-series of low nickel, austenitic grades was developed further in the 1950's when the cost of using nickel was particularly high.[2] More recent improvements in melting practices have allowed the controlled addition of increased amounts of nitrogen – a potent austenite former. However, all the low nickel austenitic grades commercially available today still contain some deliberate additions of nickel.[3] An important feature of these grades is that the reduction in nickel content cannot be completely replaced by manganese and nitrogen, with the result that the chromium content must also be reduced in order to maintain the austenitic structure. As we will see below, this side effect reduces the corrosion resistance of these alloys compared with the standard 300-series nickel grades.

One feature of all the austenitic grades is that they are not ferromagnetic at room temperature – except sometimes when cold-worked. This is of advantage in some applications where magnetism is undesirable. But a further significant benefit is that austenitic end-of-life scrap can readily be segregated by simple magnetic separation. Nickel is the most valuable element which is being recycled and, when the majority of austenitic stainless steels were 300-series, their recycling was simple. However, when 200-series scrap is mixed in with 300-series, recycling of the valuable nickel component is more complex.[3]

As the total content of austenite formers is reduced, the structure changes from austenite to a mixture of austenite and ferrite (body centred cubic). These are the duplex stainless steels. All the commercially important duplex grades, even the "lean duplexes", contain about 1% or more nickel as a deliberate addition. Most duplex stainless steels have higher chromium contents than the standard austenitic grades. Compared with the overall composition, the ferrite phase is enriched in ferrite-stabilising elements, and the austenite phase is enriched in the austenite-stabilising elements. The austenite phase may have 6-10% less chromium than the overall value, and be enriched in nickel by 20%-40%. There is some minimum nickel content necessary to

ensure solubility of these levels of chromium: the higher the mean chromium level, the higher the minimum nickel content must be. This is similar to the case for the 200-series noted above.

With the ferritic stainless steels, nickel is known to lower the ductile-to-brittle transition temperature (DBTT), i.e. the temperature at which the alloy becomes brittle. Chromium has the opposite effect, and some of the superferritic alloys can easily have a DBTT well above 20 °C. The DBTT is also a function of other factors such as grain size and other alloying additions. Some of the superferritic grades contain an intentional addition of nickel to improve the DBTT, especially of welds.

The martensitic grades are hardenable by heat treatment. Some contain nickel which not only improves toughness but also allows a higher chromium content giving increased corrosion resistance.

Finally, the precipitation hardening grades can develop very high strength by heat treatment. There are various families of PH grades but all are nickel-containing.

Formability

The face centred cubic metal structure of the nickel austenitic stainless steels gives them good tensile ductility and very good formability, as reflected in comparative forming limit diagrams. The common 18%Cr, 8%Ni grade shows particularly good stretch forming characteristics but has a somewhat lower limiting drawing ratio than some ferritic grades. Slightly higher nickel contents increase the stability of the austenite further and reduce the work hardening tendency, so increasing suitability to deep drawing. Unlike the low nickel, high manganese grades, they are not prone to delayed cold cracking.[3] This good formability has led to the widespread use of 300-series austenitic grades for items with demanding formability such as kitchen sinks, pots and pans.

Figure 2. Deep drawn double sink, courtesy, Stala.

Weldability

Many pieces of equipment have to be fabricated by welding. There are significant differences in weldability between stainless grades of any particular structural family, especially between low alloyed and high alloyed grades. However in general, the nickel austenitic grades have better weldability than other types.[4] Unlike the ferritic grades, they are not prone to embrittlement as a result of high temperature grain growth and the welds have good bend and impact properties. They are also more weldable in thick sections – say above 2 mm.

Whilst the austenitic grades have lower thermal conductivity and higher thermal expansion than other grades, these differences can be accommodated by suitable fabrication practices. As a

result, nickel-containing grades such as Types 304 and 316 are the most widely fabricated stainless steels around the world.
The duplex grades are far more weldable than the ferritic grades for equivalent alloy content, but even the standard and superduplexes require more attention to the details of the welding procedure than the equivalent austenitic grades. The 200-series alloys have welding characteristics most similar to the 300-series alloys.

Toughness

Toughness – the ability of a material to absorb energy without breaking - is essential in many engineering applications. Most stainless steels have good toughness at room temperature but with decreasing temperature, the ferritic structure becomes progressively more brittle so that ferritic stainless steels are not suitable for use at cryogenic temperatures. In contrast, the common austenitic stainless steels retain good toughness even to liquid helium temperatures, so grades such as Type 304 are widely used for cryogenic applications.

High Temperature Properties

The addition of nickel provides the austenitic grades with significantly better high temperature strength – particularly the ability to resist creep – than other grades. These grades are also much less prone to embrittlement at room temperature as a result of exposure at intermediate and high temperatures which may cause the formation of deleterious phases. Nickel also promotes the stability of the protective oxide film and reduces spalling during thermal cycling. Consequently, the austenitic grades are used for high temperature applications and where fire resistance is needed. It is worth noting that there is a continuum in composition between the austenitic stainless steels and the nickel-based superalloys, which are used for the most demanding high temperature applications such as gas turbines.

Corrosion Resistance

As already discussed, it is the formation of the chromium-rich oxide layer which is at the heart of the corrosion resistance of stainless steels. However, particularly in the presence of chlorides, this layer is susceptible to damage which can lead to the onset of localised corrosion such as pitting and crevice corrosion. Stainless steels are often ranked for their resistance to the initiation of such localised corrosion by the Pitting Resistance Equivalent (PRE):

$$PRE = Cr\% + 3.3Mo\% + 16N\%$$

Both molybdenum and nitrogen increase resistance to pit initiation in the presence of chlorides. Nickel does not appear in the equation but nickel is important in reducing the rate at which both pitting and crevice corrosion propagate after initiation, see Figure 3.

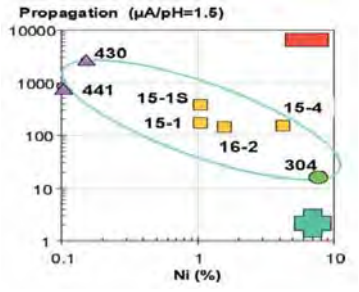

Figure 3. Beneficial effect of nickel in reducing the propagation rate of pitting and crevice corrosion.[3]

Nickel also influences the resistance of stainless steels to another form of localised corriosion, chloride stress corrosion cracking. In this case however, there is a minimum in resistance at

nickel contents of around 8%: stress corrosion cracking resistance increases markedly at nickel levels which are both lower and higher than this.

In general, increasing the nickel content of stainless steels, including ferritic grades, also increases their resistance to reducing acids like sulphuric acid. Other elements such as molybdenum and particularly copper also have a strong influence in this regard.[5] However, there are potential drawbacks to using nickel in this way in the ferritic grades, related to stress corrosion cracking resistance and formation of intermetallic phases.

Lustre

At first sight, all stainless steel grades look similar. However, side-by-side comparisons of identical surface finishes do show differences in colour and lustre. Appearance and aesthetic qualities will always be a matter of taste but the 200-series grades can seem darker and the ferritic grades cooler in appearance than the nickel austenitic grades. In some architectural applications, a grayer colour might be preferred, but generally consumers prefer a brighter, whiter metal, as witnessed by the popularity of the 300-series.

Choosing the right grade

How is a design engineer to select the most appropriate grade of stainless steel from the range available? Choosing an alloy with suitable corrosion resistance for the expected service is a good starting point. That alloy should have a sufficient margin of safety to allow for excursions which might occur outside the normally expected operating conditions since an operator may want to push a plant to deliver higher throughputs by use of higher temperatures and pressures than were allowed for in the original design.

As the trend towards risk-based inspection increases, a higher corrosion resistance can be used to justify a reduced inspection frequency. The combination may lower overall cost. Process equipment downtime is often overlooked but can be a very expensive side effect of choosing an inadequate material. Furthermore, equipment failure may cause release of harmful chemicals which can have a severe human or environmental impact - with consequent legal repercussions. For all these reasons, it is rarely good practice to select a grade which is only just capable of resisting the design environment.

A conservative approach to selection for corrosion resistance can also be justified where maintenance of product purity is paramount, such as in the food and pharmaceutical industries.

For many applications, mechanical properties are not critical, for example, purely decorative architectural uses. However, when mechanical properties are an important design consideration, it may be possible to take advantage of the higher strength of cold worked austenitic grades or the duplex grades in order to reduce the total weight and hence overall cost of the material used. Lighter weight may also lead to lower installation and support structure costs.

Fabricability is an important consideration for many applications whether in buildings, chemical plant or consumer items. This may apply not just to the material characteristics but also to the level of welding skill needed. This alone may rule out less fabricable grades in some applications and it is the excellent fabrication characteristics of the austenitic stainless steels which often leads to their selection.

There are many situations where specific physical properties are required which then restricts the grades under consideration. For example, low magnetic permeability austenitic stainless steel must be used in a MRI (magnetic resonance imaging) facility.

Ready availability of material in all the necessary forms for a project can be a major consideration. That is where the established "commodity grades", such as Types 304 and 316, can have a distinct advantage because they are stocked very widely. This is unlikely to be the case with more specialised, proprietary grades until they have become well-established. A related point is the familiarity which suppliers, fabricators and users have with the long-established, widely used grades. It is another reason why the majority of applications are still satisfied by a handful of grades.

There is increasing emphasis on selecting materials which contribute to a low environmental impact. This should be seen in a broad context, which covers not only the raw materials and end-of-life recycling credits but also the contribution to reduced environmental impact throughout the operating life of the project. For example, reduced energy consumption as a result of improvements in process efficiency may be far more important than the energy content of the raw material.

Only when the above requirements have been evaluated and satisfied should cost considerations be used to make the final material selection. And the appropriate tool to use then is full life cycle costing. Even among materials that are otherwise suitable property-wise, the least expensive initial cost material may well be a much more expensive choice in the long term. For these reasons, nickel is almost certain to remain a major alloying element in stainless steels for the foreseeable future.

References

[1] R. A Covert and A. H. Tuthill: "Stainless Steels: an Introduction to their Metallurgy and Corrosion Resistance", Dairy, Food and Environmental Sanitation, Vol 20, No 7, pp 506-517, reprinted as Nickel Institute publication 14056.

[2] R. E. Paret: "Fabrication of Low-Nickel, High-Manganese Stainless Steels" and "Experience with High-Manganese Stainless Steels", Metal Progress, May and June, 1956, reprinted as The International Nickel Co. Inc publication number 223.

[3] J. Charles: "The new 200-series: an alternative answer to Ni surcharge? Dream or nightmare?": Stainless Steel '05 Science and Market, Seville 2005, ed. Odriozola & Paúl, pp 19-27.

[4] "Welding of Stainless Steel": Euro Inox Materials and Application Series, Vol 3.

[5] U. Heubner: "Nickel alloys and high-alloy stainless steels – materials summary and metallurgical principles", Nickel alloys and high-alloy special stainless steels, 2nd edn, 1998, Krupp VDM.

A NEW EUROPEAN 200 SERIES STANDARD TO SUBSTITUTE 304 AUSTENITICS?

J. Charles[1], J.D. Mithieux[1], J. Krautschick[2], N. Suutala[3], J. Antonio Simón[4], B. Van Hecke[5], T. Pauly[6]

[1]ArcelorMittal Stainless, France, [2]ThyssenKrupp Stainless,Germany, [3]Outokumpu, Finland, [4]Acerinox, Spain, [5]ArcelorMittal Stainless, Belgium, [6]Euro-Inox, Belgium

Abstract

A new grade of the 200 series has been defined for the European market as a candidate alternative to austenitic grade EN 1.4301 (AISI 304). It has been designed for certain applications at the lower end of the corrosion resistance range of this reference material. A new chemistry has been proposed to ensure adequate properties as there had been disappointment in the European market with poorly defined imported products. The new grade is designed to reduce the nickel content (to min 4.5%) while still stabilising the austenitic phase with combined copper (min. 1%) and relatively low nitrogen and carbon contents. A minimum of 16.5% Cr combined with 0.1% N and 1% min. Cu provide the required corrosion resistance properties while copper additions make it possible to improve drawability. The grade was recently assigned a material number by VDEh (1.4618 – X9CrMnNiCu 17-8-5-2). The paper presents mechanical properties of the grade including drawability and corrosion resistance characteristics. Experimental data of the newly designed grade are compared to the existing 200 grades as well as to stainless steels of the 300 and 400 series. It is concluded that the newly designed grade has mechanical properties slightly superior to those of EN 1.4301 (AISI 304) and equivalent to those of EN 1.4310 (AISI 301) grade. In terms of corrosion resistance, the grade is close to that of grade EN 1.4301 (AISI 304), upgrading the classical 200 series.

Introduction

For more than 50 years manganese additions have been considered as a replacement of nickel in austenitic stainless steels. As a result, reductions in alloy surcharge, particularly at times of nickel prices peaks, can be expected. This has resulted in the development of the so-called 200 series. The grades are known to have complementary nitrogen additions in order to further stabilize the austenitic phase. Copper additions have also been successfully considered in order to provide a stable austenite. With copper additions, nitrogen additions can be reduced providing softer manganese austenitic grades.

The grades had only limited applications - with a few exceptions, such as India - until the end of the last century. They were selected mainly for their combination of high strength and ductility. More recently large amounts of type 200 stainless steels have been produced in Asia. The grades show modified chemical compositions – low chromium additions, extra low nickel additions ... – and in some cases high residual elements like sulfur which are known to have detrimental effects on localized corrosion resistance (pitting, crevice).

The lack of international standards and references for those grades has been pointed out recently. Grades in coils or finished products have been imported into Europe without clear references.

They are called equivalent to 304 regardless of their chemistry. In some cases they have been labeled 18-10 grades or even 300Mn series.
For a European 200 series to be viable, a certain amount of standardization was required. Providing technical information was made a priority to avoid misunderstandings and improper use of poorly defined type 200 stainless steels. There was an urgent need to avoid damage to the excellent image of stainless steels.
In order to fulfill these requests, a working group with representatives of the main European flat stainless steel producers was created under the umbrella of Euro-Inox. The main conclusions are presented in this paper.

History and current developments in the 200 series

The 200 series of stainless steels was developed in the early 1930s. Although the first chemical analyses investigated were of the 205 kind (Ni content close to 1% and stabilization of the austenitic phase by simultaneously high manganese and nitrogen additions - see figures 1 and 2), the first grades which received the AISI label in the mid-fifties were the 201 and 202 grades (Ni content around 4 to 6 % and nitrogen additions lower than 0.25 %). They became more popular out of the urge to conserve the nickel during the Korean War. In that time, nickel uses were mainly restricted to military applications. The Tenelon grade / AISI 214 grade with less than 2% Ni and about 0.35%N was produced at the end of the fifties. The Mn-austenitic grades containing Mo to improve the corrosion resistance properties appeared in the mid-sixties both in the US and Europe.
Simultaneously Mn and Cu containing grades were developed which made it possible to produce 4 to 6 %Ni austenitic grades (AISI 211 and 203) with relatively low nitrogen content (< 0.06 %). Equivalent drawing properties to 304 could be achieved. Due to a new Ni shortage phenomenon, the grades started to be popular in the early 70's. With the new AOD technology, nitrogen additions in the 200 series were made easier and more cost-effective (Table 1). Once again nickel shortage ended and with high availability, Ni prices went down again. For more than 30 years, grade 304 was the standard of the stainless steel family at an average yearly growth of 5 to 6%.

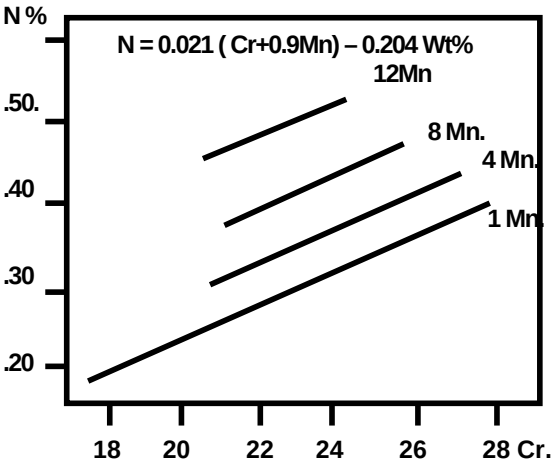

Figure 1. Effects of %Cr and %Mn on N solubility

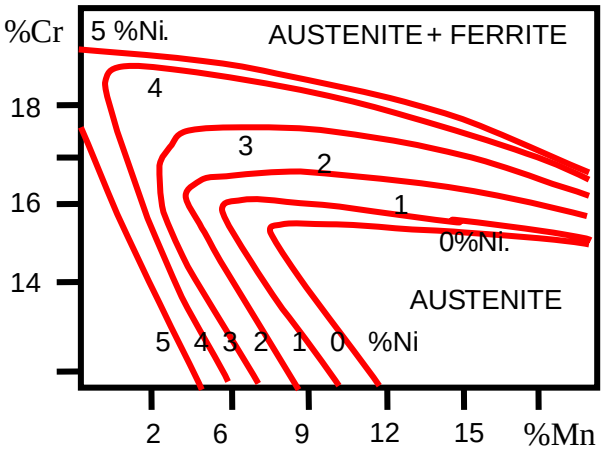

Figure 2. Aust. stability at 1075°C (Franks)

The 200 series still had marginal applications in the eighties and nineties. With the new century, a new period of high volatility of nickel price started. Asia and particularly China became a major consumer of stainless steel. Part of the tonnage was produced locally, the remaining being imported mainly from India.

Table 1. Chemical analyses of different 200 series grades.

Type	Standard	Cr	Ni	Mn	N	C	S	OTHERS
201	S20100	16.0 - 18.0	3.5 - 5.5	5.5 - 7.5	0.25MAX	0.15MAX	0.030MAX	-
201LN	S20153	16.0 - 17.5	4.0 - 5.0	6.4 - 7.5	0.10 - 0.25	0.03MAX	0.015MAX	Cu 1.0MAX
202	S20200	17.0 - 19.0	4.0 - 6.0	7.5 - 10.0	0.25MAX	0.15MAX	0.030MAX	-
204L	S20400	15.0 - 17.0	1.5 - 3.0	7.0 - 9.0	0.15 - 0.3	0.03MAX	0.030MAX	
	S20430	15.5 - 17.5	1.5 - 3.5	6.5 - 9.0	0.05 - 0.25	0.15MAX	0.030MAX	Cu 2.0 - 4.0
205	S20500	15.5 - 17.5	1.5 - 3.5	14.0 - 15.5	0.32 - 40	0.12 - 0.25	0.030MAX	
214	S21400	17.0 - 18.5	1.0MAX	14.0 - 16.0	0.35MIN	0.12MAX	0.030MAX	
216	S21600	17.5 - 22	5.0 - 7.0	7.5 - 9.0	0.25 - 0.5	0.08MAX	0.030MAX	Mo 2.0 - 3.0
	S24000	17.0 - 19	2.25 - 3.75	11.5 - 14.5	0.2 - 0.4	0.08MAX	0.030MAX	
	S32001	19.5 - 21.5	1.0 - 3.0	4.0 - 6.0	0.05 - 0.17	0.03MAX	0.030MAX	Cu 1.0MAX
	EN 1.4371	16.0 - 17.0	3.5 - 5.5	6.0 - 8.0	0.15 - 0.20	0.03MAX	0.015MAX	-
	EN 1.4372	16.0 - 18.0	3.5 - 5.5	5.5 - 7.5	0.05 - 0.25	0.15MAX	0.015MAX	
	EN 1.4373	17.0 - 19.0	4.0 - 6.0	7.5 - 10.5	0.05 - 0.25	0.15MAX	0.030MAX	

The continuous pressure to obtain low cost grades resulted in the development of cheaper stainless steels with lower and lower amounts of alloying elements such as nickel and even chromium. Due to low cost and sometimes less performing manufacturing routes grades with very high sulfur and carbon were sold on the market. Such productions moved from a marginal level to hundreds of thousands of tons. Typical 200 series chemistries including more recently developed grades are presented in Table 2. As observed some of the grades (X1, X2) have very low Cr and high sulfur contents.

Table 2. Typical chemistries of 200 series (X1, X2 samples issued from Asian market).

Country	Cie	Usual name	UNS	Cr	Ni	Mn	Cu	C	N	S (ppm)	Rp0.2	Rm	Md
Europe	U&A	16-4Mn	S20100	16,3	4,1	6,5		0,09	0,16	40	400	770	39,99
	U&A	16-7Mn †	S20400	16	1,6	7,5	2,9	0,05	0,19	< 10	390	710	28,92
	KTN	H400		18	3,8	6,8		0,035	0,16	7	450	770	48,35
USA		Nitronic 30	S20400	16	2,5	8,5		0,02	0,17		390	830	101,8
		Nitronic 19D *	S32001	20	1,6	5	0,5	0,02	0,13		500	850	105,8
	Allegheny	219	S21904?	21	6	9		0,03	0,25		460	780	-114
S.Amer.	Acesita	P201A	-	15,2	1,1	9	1,7	0,1	0,1	<10	370	870	95,36
	Acesita	P202A	-	15,1	4	7,2	1,6	0,06	0,05	<10	310	730	71,87
	Acesita	P300A †	S20400	16,1	1,5	7,4	2,9	0,05	0,18	3	370	745	35,89
Asia	Jindal	J1	-	15	4	7	1,6	0,06	0,05	60	300	700	74,88
	Jindal	JI	-	16,1	4	7,1	1,7	0,06	0,07	31			46,85
	Jindal	J4	-	15,5	1	10	1,6	0,09	0,14	60	470	820	74,99
	Jindal	J4	-	15,9	1	9,7	1,6	0,1	0,15	82			62,73
	NTK	D10	-	17,5	4,8	3,7	2,8	0,06	0,15	10	355	675	-36,5
	X1	-	-	15	1,1	9,6	1,7	0,1	0,14	123			74,7
	X2	-	-	11,3	1,1	12,8	0,08	0,13	0,045	60			176,2

The new 200 European grade: 1.4618

The newly developed type 200 grade is designed to obtain an optimum compromise between cost reduction (lower nickel), high formability properties (reduced C, N additions but with Cu) and corrosion resistance properties as close as possible to 304 (16.5% Cr min; 4.5% Ni min).
Table 3 presents the 1.4618 specification, which has been agreed by the main European stainless producers. The grade meets the 201-1 “rich side” of the AISI 201 specification.
As observed, the grade can be considered as a “soft” representative of the 200 series. In the second half of 2007, more than 1,000 tons issued from industrial melts were delivered to European and American markets. Typical mechanical properties of those production lots are

presented in Table 4. The grade behaves like a 301 austenitic steel, i.e. mechanical properties (YS) are slightly higher than those of grade EN 1.4301 (AISI 304).

Table 3. VDEh 1.4618 specification.

Steel number	1.4618
Steel name	X9CrMnNiCu17-8-5-2
Chem. Composition in % by mass	C ≤0.10, Si ≤1.00, Mn 5.50-9.50, P ≤0.070, S ≤0.010, Cr 16.50-18.50, Ni 4.50-5.50, Cu 1.00-2.50, N ≤.15
YS 0.2% (MPa)	220
UTS (MPa)	520-850
El 80 % min.	40
KV 20 °C (Joules)	100

The composition of the grade starts from he requirements of EN 1.4372 and AISI 201. Copper addition is necessary for metallurgical reasons in order to obtain mechanical properties close to those of grade EN 1.4301 (AISI 304). Its mechanical properties are in accordance with the AISI 201-1 “rich side”, but are too soft for the EN 1.4372 or AISI 201-2 “lean side”.
It will be included at the next revision of EN10088 under the number 1.4618 and for the time being certificates can be supplied from the mills according to ASTM A240 grade 201-1 and the agreement of the customer upon copper addition.

Table 4. ASTM and European Standard equivalences.

	UNS	Type		C	Mn	P	S	Si	Cr	Ni	N	Cu
ASTM A240	S20100	201		0.15	5.5-7.5	0.060	0.030	1.0	16.0-18.0	3.5-5.5	0.25	
EN 10088-2	1.4372	X12CrMnNiN17-7-5		0.15	5.5-7.5	0.045	0.015	1.0	16.0-18.0	3.5-5.5	0.05-0.25	
	1.4618	X9CrMnNiCu17-8-5-2		0.10	5.5-9.5	0.07	0.010	1.00	16.5-18.5	4.5-5.5	0.15	1.00-2.50
	1.4618	201.1 Cu		0.03-0.065	5.6-6.4	0.035	0.0020	0.5	16.6-17.2	4.4-5.0	0.070-0.110	1.4-1.8

				UTS min		YS min		E% min		Hardn. Max		KV ep>10 mm	
	UNS	Type		ksi	MPa	ksi	MPa	2" 50 mm	80 mm	HB	HRB	L	T
ASTM A240	S20100	201-1 "rich side"		75	515	38	260	40		217	95		
		201-2 "lean side"		95	655	45	310	40		241	100		
EN 10088-2	1.4372	X12CrMnNiN17-7-5	C		750-950		350		45				
			H		750-950		330		45			100	60
	1.4618	X9CrMnNiCu17-8-5-2			520-850		220		40			100	
		Typical values 2B			650		330		50		87		

Mechanical Properties

Table 5. Mechanical properties.

Producer	TEMP.	Thickness	Rp0.2	Rp1.0	Rm	A8)	r
	°C.	mm.	Mpa	Mpa.	Mpa	%	
TKI	20	0.4	304		663	58	0.9
	20	0.5	309		660	55	0.87
	20	2.5/4.5	345		653	50	
OUTOKUMPU	20	1/2	318	351	652	50	
	150	1	218	252	530	50	
	350	1	174	210	494	39	
	350	0.6	186	215	508	38	
ArcelorMittal	20	3	325		645	56	0.93
	20	HRAP 5	343		650	52	1

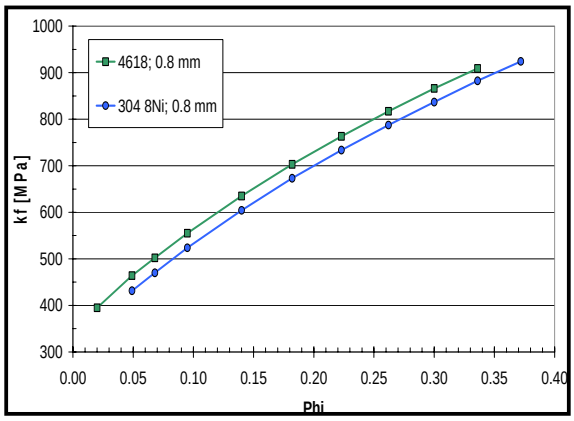

Figure 3. Rp0.2 versus cold reduction (3048Ni)

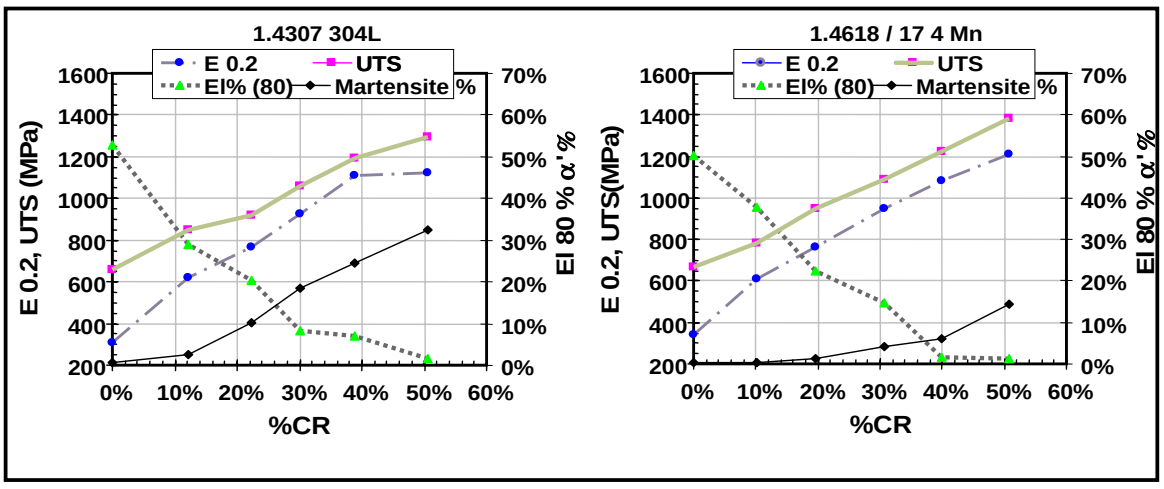

Figure 4. Austenitic stability and mechanical properties versus cold reduction.

When cold worked, grade 1.4618 has less α-martensite than grade EN 1.4307 (AISI 304L) for a given deformation. Mechanical properties remain very similar even if the 1.4618 grade shows slightly higher mechanical properties in the cold worked state, compared to EN 1.4307 (AISI 304L). Figure 5 illustrates that 1.4618 is a much softer grade than EN 1.4372 (AISI 201) whereas ferritic grade 1.4509 (441) behaves differently.

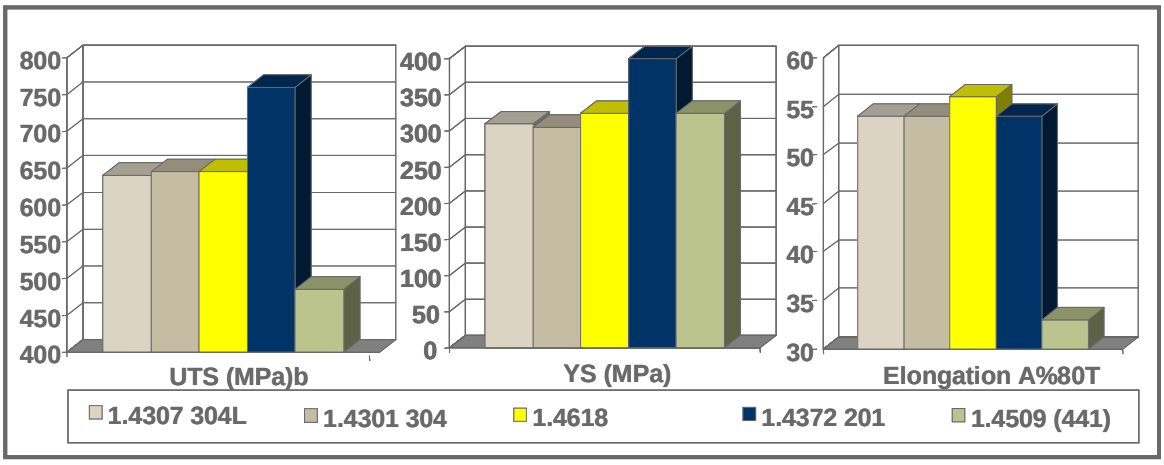

Figure 5. Room temperature tensile properties of several austenitic and ferritic stainless steels.

Figure 6. 1.4618 toughness results

a)

Drawing tests	Thickness	K50	K100	LDR
1.4618	0.4	30.8	59.6	2.03
TK	0.8	33.0	64.0	2.00
TK 304 8Ni typ. Val.	0.8	33.9	66.1	2.06

• Delayed cracking→ No cracks up to β = 2.03 (comparable to 304 8Ni)

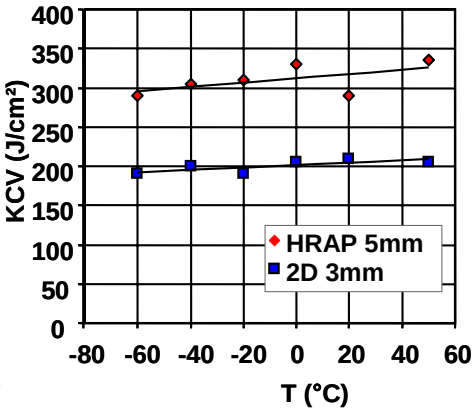

2D 3mm

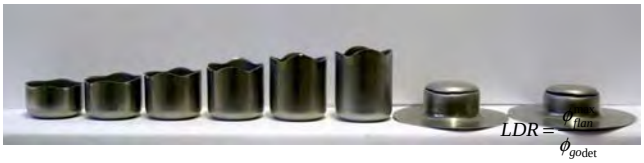

Expansion Erichsen

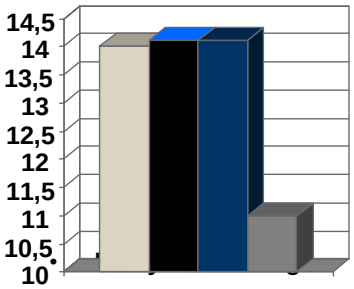

b)

1.4307 304L
1.4618
1.4372 201
1.4509 441

201 more sensitive to Delayed cracking

LDR- Limit Drawing Ratio

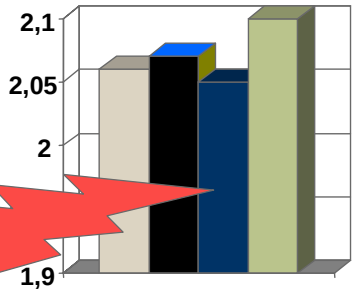

◊ no cracks (Swift cup b = 2.05) ; Bending test: No defect (bending radius 4 mm)

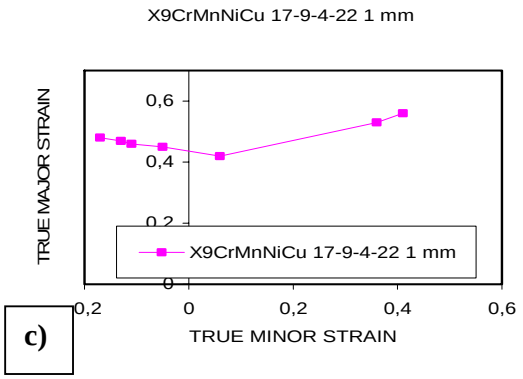

% FLD data - 705-1 Th : 1.0 mm		
% Width [mm]	Minor strain (e2)	Major strain (e1)
20	-0,17	0,48
40	-0,13	0,47
60	-0,11	0,46
100	-0,05	0,45
120	0,06	0,42
140	0,36	0,53
200	0,41	0,56

Figure.7. Formability results

Grade EN 1.4618 performs at least as well as grade EN 1.4307 (AISI 304L) in terms of formability. As for all austenitic structures, expansion properties are excellent. LDR values are improved when compared to the classic grade EN 1.4372 (EN201) grades. This is also the case for delayed cracking behaviour. Obviously the combination of minimum 1% Cu additions and optimum nitrogen content significantly improves the formability properties of grade 1.4618, when compared to the other 200 series grades.

Corrosion Resistance Properties

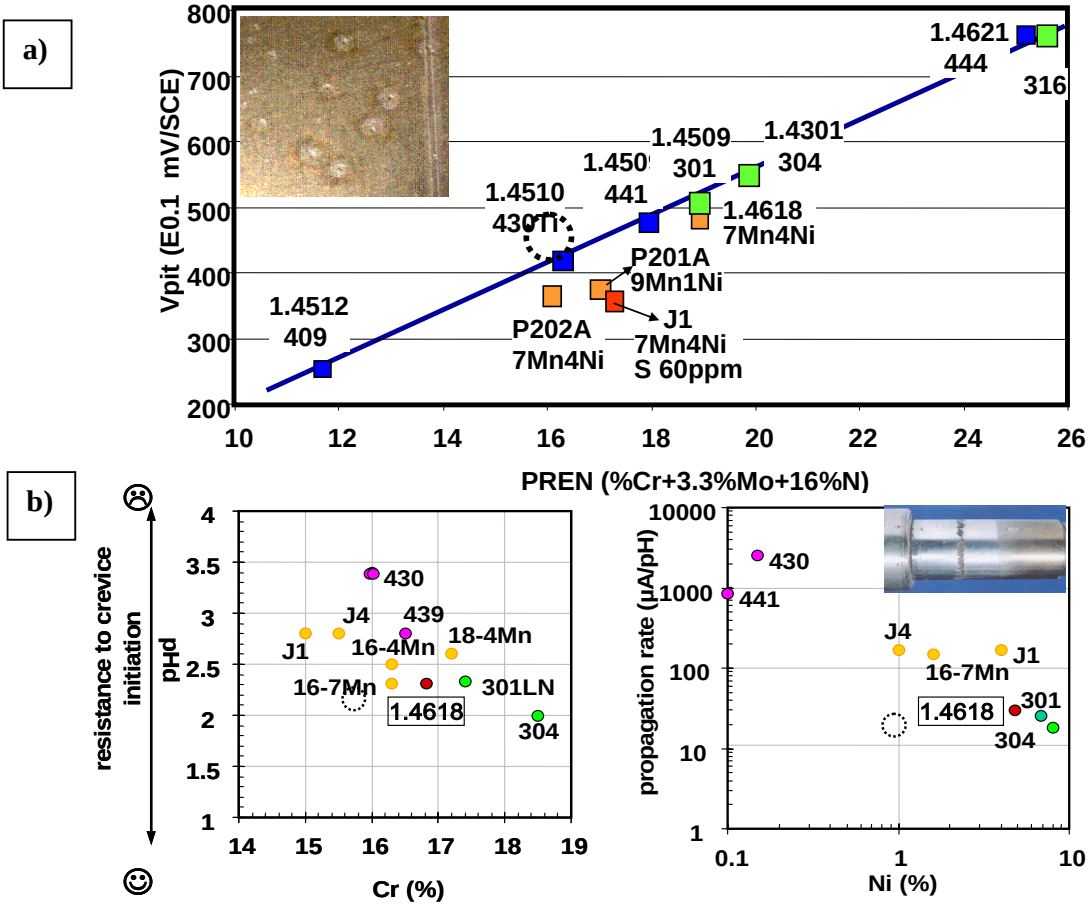

Figure 8. a) Pitting corrosion resistance properties (critical pitting potentia,pH = 7).
b) Crevice corrosion resistance properties (pHd in NaCl 2M, T= 23°C sol.)

Pitting corrosion resistance of grade 1.4618 has been investigated by potentiodynamic curves performed in a 0.02M NaCl (23°C - pH 7) solution (Figure 8a). The grade behaves like grade EN 1.4310 (AISI 301), i.e. its pitting corrosion resistance is slighly lower that that of the austenitic grade EN 1.4307 (AISI 304L). This results from a slight reduction in Cr content partially compensated by N additions which enhance pitting corrosion resistance properties. Considering crevice corrosion resistance, grade 1.4618 again has equivalent properties to a EN 1.4310 (AISI 301) austenitic stainless, whose behavior is very close to that of grade EN 1.4307 (AISI 304L). Considering crevice corrosion propagation, Ni has a powerful effect in reducing the corrosion rate. At 4.5%Ni, the 1.4618 grade has much better properties than 1% Ni 200 series grades. For both pitting and crevice corrosion resistance, grade 1.4618 is the best performing grade among the 200 series grades investigated.

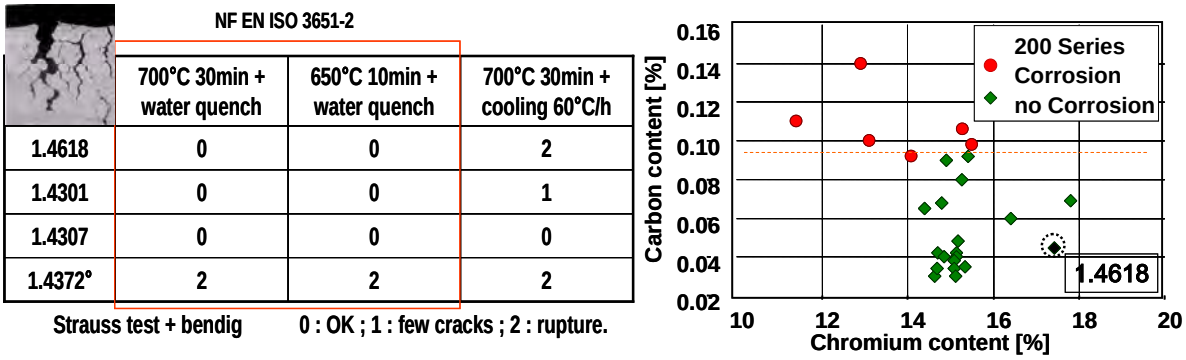

Figure 9. Intergranular corrosion resistance results. Beneficial effects of reducing C and N contents.

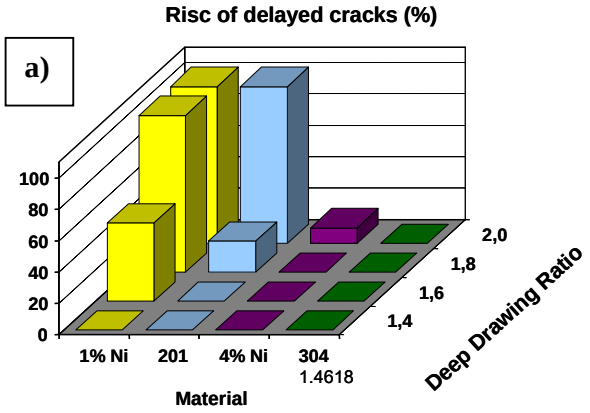

Figure 10. a) Delayed cracking results
b) SCC tests on caps (salt spray tests).

Cap results after 1000 H Exposure –(ASTM B117) : Salt spray testsNbr of cup with cracks.

b)

Grade	Drawing ratio	Nb. of cracks
1.4301	1,83	0/3
	1,94	0/3
304DDQ	1,83	0/3
	1,94	2/3
1.4618	1,83	2/3
	1,94	3/3

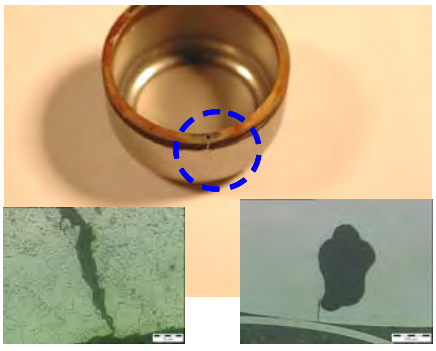

Intergranular corrosion resistance was investigated by means of Strauss tests followed by bending tests. Drastic improvements are observed compared to grade EN1.4372 (AISI 201). Reducing nitrogen and carbon contents improves the behavior of the steel. Only sensitising treatments at 700°C for 1 hour may induce intergranular cracks after Strauss test and bending operations. In those conditions even grade EN 1.4301 (AISI 304) is sensitised. In all testing conditions grade EN1.4372 (AISI 201) has the poorest behavior.

Delayed cracking properties are also markedly improved by this chemistry. The grade performs almost like grade EN 1.4301 (AISI 304). Salt spray tests performed on caps have shown, for the most critical areas, crack propagations for grade 1.4618 which are not observed for type EN 1.4301 (AISI 304) grades. Metallographic investigations have identified that mostly cracks initiate on corroded areas (small crevice; pitts,…). This is consistent with results presented earlier showing a slight decrease in localised corrosion when comparing grade 1.4618 to grade EN 1.4301/304L.

Weldability

Table 6. Typical 1.4618 welding conditions.

Welding process	Without FM	With Filler Metal			Protective Gas
	Typical Thickness	Thickness	Filler Metal		
			Wire rod	coil	
Spot welding Seam weld	< 2 mm < 2 mm				
TIG	< 1.5 mm	> 0.5 mm	ER 308 L (Si) W.Nr 1.4370 ER 347 (Si)	ER 308 L (Si) W.Nr 1.4370 ER 347 (Si)	Argon Argon + 5 % Hydrogène Argon + Hélium
PLASMA	< 1.5 mm	> 0.5 mm	ER 310	ER 308 L (Si) W.Nr 1.4370 ER 347 (Si)	Argon Argon + 5 % Hydrogène Argon + Hélium Argon + 2 % C02
MIG		> 0.8 mm		ER 308 L (Si) W.Nr 1.4370 ER 347 (Si)	Argon + 2% 02 Argon + Hélium Argon +3%C02+ 1 %H2
S.A.W.		> 2 mm		ER 308 L ER 347	
Électrode		Repairs'	E 308 E 308 L E 347		
Laser	< 5 mm				Helium Restricted : Argon - N2

Typical welding conditions for grade 1.4618 are presented Table 6. The grade behaves almost like grade EN 1.4301 (AISI 304). No specific welding parameters have to be used in most of the cases. EN 1.4301 (AISI 304) or EN 1.4310 (AISI 301) welding products may be used.

Conclusion

Extensive data of the newly designed 1.4618 grade have been presented. It is concluded that the grade for a 200 series grade has an optimum chemical composition to obtain mechanical and corrosion resistance properties equivalent to those of grade EN 1.4310 (AISI 301).
Deep drawing properties can be obtained without significant sensitivity to cold cracking phenomena. The grade has a weld ability equivalent to those of grade EN 1.4301 (AISI 304).
The grade is designed to offer to end-users a 200 series grade able to replace 304-like grades in a wide number of cases. Nevertheless, for the most severe conditions, 1.4618 grade is slightly more sensitive to corrosion phenomena than 304 grade.

The grade has been jointly developed with ArcelorMittal Stainless, ThyssenKrupp Stainless, Outokumpu and Acerinox under the umbrella of Euro-Inox.

Acknowledgements

Grateful acknowledgement is made to ISSF who through the marketing committee chaired by JY Gilet sponsored the first international team to collect data on “200-series” steels. The authors thank JY Gilet and Staffan Malm for there continuous support. Part of the work is issued from experimental data presented in ISSF document (main work performed by Dr Sindhal – Jindhal-, Dr J. Krautschick –TKS- and Dr J. Charles – ArcelorMittal Stainless Europe).

References

[1] ISSF 05 document: “New 200-series” steels: an opportunity or a threat to the image of stainless steel? Technical guide to chrome-manganese austenitic stainless steels and advice for potential users.

[2] J. Charles: The new 200-series: an alternative answer to Ni surcharge? Stainless Steel USA Int.conf, 2006, Houston.

OPTIMIZATION OF THIN STRIP CAST AUSTENITIC 304 STAINLESS STEEL MICROSTRUCTURES

D. Raabe[1], B. Sander[1], R. Degenhardt[2], R. Sellger[2], W. Klos[2], M. Sachtleber[2], L. Ernenputsch[2]

[1]Max-Planck-Institut für Eisenforschung, Germany, [2]ThyssenKrupp Nirosta GmbH, Germany

Abstract

We present recent results about the optimization of the microstructure and properties of thin strip cast austenitic stainless steel (AISI 304, 1.4301). Concerning the processing steps the relevance of different thin strip casting parameters, in-line forming operations, and heat treatments for optimizing microstructure and properties have been studied. The microstructures obtained from the different processing strategies were analyzed with respect to the phase and grain structures including the grain boundary character distributions via EBSD microtexture measurements, the evolution of the deformation-induced martensite, the relationship between the delta ferrite and martensite formation in the austenite, and the texture evolution during in-line deformation. It is observed that different process parameters lead to markedly different microstructures and profound differences in strip homogeneity. It is demonstrated that the properties of strip cast and in-line hot rolled austenitic stainless steels are competitive to those obtained by conventional continuous casting and hot rolling in the annealed and pickled state.

Introduction

Stainless steel strips are conventionally manufactured by continuous casting, slab reheating, hot rolling, hot strip annealing, and pickling. Thin strip steel casters offer a competitive efficient alternative to industrially produce such steels when compared to the conventional thick-slab production lines. Current advanced twin roll thin strip casters for the production of stainless steels combine the two operations of casting liquid metal between two rolls and subsequently imposing in-line hot deformation steps to produce hot rolled thin strips that are directly coilable [1-5], Figure 1. Twin roll thin strip casting of steels thus eliminates major steps required in conventional production, for instance slab handling, slab reheating, hot strip roughening / break-down reversing rolling, and hot rolling in a conventional hot rolling mill (set of 5-7 four-high stands), Figure 2. Both, thin strip cast material and conventionally produced hot strips can be further cold rolled and recrystallization annealed, depending on the desired final thickness and properties. Thin strip casting of stainless austenitic steel (AISI 304 / 1.4301 in this work) provides a number of significant advantages in comparison to the conventional slab processing method. First, the thin strip casting method permits the entire continuous conventional hot rolling process to be bypassed. The thin strip casting method is even capable of producing strips with a smaller thickness than conventional production routes. At the same time is allows one to produce steel strips which are difficult to be cast or hot rolled by conventional methods, such as for instance some complex highly alloyed austenitic grades. Second, it offers a significantly higher solidification rate which leads to microstructures with reduced dendrite arm spacing, reduced microsegregations, and smaller inclusion sizes when compared to conventional slabs. Third, the thin strip route allows exploiting higher and locally different heat fluxes which may lead to alternative solidification modes with respect to the primary γ / δ phase ratio close to the strip of

the surface. Fourth, the weak crystallographic texture and low through-thickness texture gradients of strip cast steels, which predetermine the forming properties and strength of the final strip, leads to reduced anisotropy when compared to conventional hot strip material [6-13]. Fifth, the microstructure and properties of strip cast austenitic 304 stainless steels are equivalent to those obtained by conventional processing. Also, strip cast austenitic stainless steels often reveal a more homogeneous microstructure through the strip thickness than conventional hot rolled material. This means that the scatter in the mechanical properties may be even lower than in the case of conventionally produced stainless steels that are known to reveal through-thickness gradients of their texture and microstructure [14-19]. Finally, the strip casting route is the most environmentally friendly, energy saving, and CO_2-sensitive way to steel. In this study we present recent advances in the optimization of the microstructure and properties of strip cast austenitic stainless steels (AISI 304, 1.4301). We discuss in part the influence of some of the relevant process parameters (e.g. coiling temperature, in-line hot rolling temperature, lubrication, in-line rolling speed, heat treatments) for optimizing the microstructure and properties of the final strips.

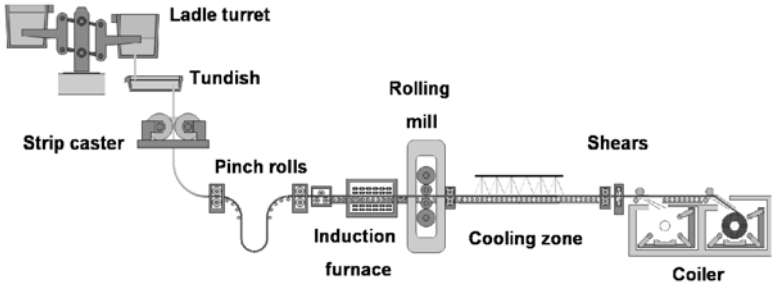

Figure 1. Schematical figure of the thin strip casting plant of ThyssenKrupp Nirosta in Krefeld, Germany.

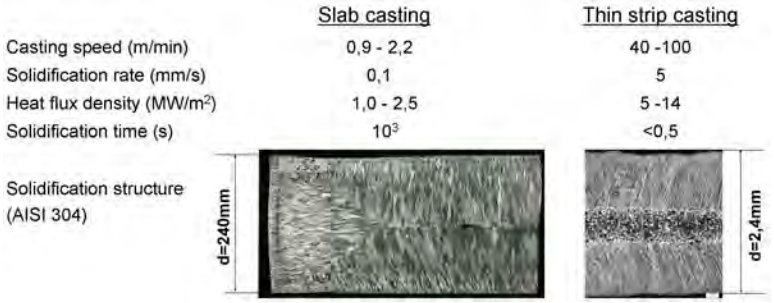

Figure 2. Relevant process parameters of the thin strip casting and the conventional hot strip route. Strip width is up to 1600mm so that up to 2.5 tons can be cast per minute.

Experimental

We investigated austenitic stainless steel with commercial analysis (~18 weight % Cr and ~8.5 weight % Ni according to AISI 304, 1.4301). The strips were cast on an industrial twin roll thin strip caster at the ThyssenKrupp Nirosta stainless steel plant in Krefeld, Germany, Figure 1. The method works by casting liquid steel into a preheated tundish, which contacts two rotating rolls which have symmetrical position and size. The steel solidifies as thin film on the roll surfaces. In the gap the films impinge and are compressed to a strip. The thickness of the strip samples typically lies between 1.5 and 3.5 mm. Subsequent deformation was conducted using a single in-line hot rolling stand, Figure 1. Specimens for microstructure characterization were cut as longitudinal sections for metallography, HR-SEM (high resolution scanning electron microscopy), EDX (energy dispersive x-ray spectrometry), and HR-EBSD (high resolution electron back scatter diffraction). The measurements were conducted on a JSM-6500F field emission SEM (15kV, 100nA). Crystallographic orientation mappings were taken using step sizes of 50nm-500nm, depending on the resolution desired. The EBSD data were used to

determine crystallographic texture, interface character, crystal size distribution, and area fractions of the coexisting phases. Details on the EBSD technique are given in [20-23].

Results and Discussion

As-cast thin strip microstructure

The optical longitudinal section of an as-cast sample reveals a microstructure which consists of uniformly oriented blocks of austenitic dendrites, Figure 3. The primary dendrite extension along the normal direction is in part up to 1 mm. In the surface region (~100µm from the surface) of the thin cast strips the microstructure is finer than below this zone. This observation indicates that growth selection takes place at the beginning of the solidification process.

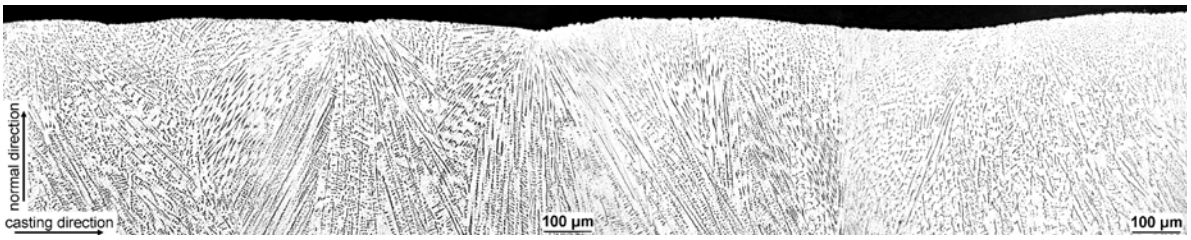

Figure 3. Longitudinal section of an as-cast 304 stainless steel sample, analyzed by optical metallography.

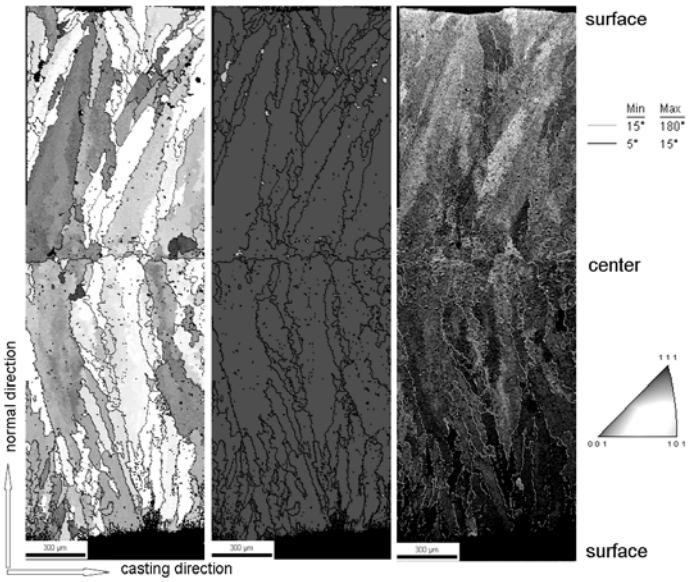

Figure 4. Longitudinal section of an as-cast thin strip sample, measured by EBSD. Left: crystal orientations in terms of their respective Miller index, {hkl}, parallel to the strip surface; Middle: distribution of the two main phases, namely of the γ austentic face centered cubic (FCC) majority phase and the finely dispersed body centered cubic (BCC) δ minority phase. Right: distribution of the grain boundary character in the same metallographic section.

Figure 4 shows a magnified part of a longitudinal section of an as-cast thin strip specimen as measured by HR-EBSD. The first image (left hand side) shows the crystals in terms of their respective Miller index, {hkl}, parallel to the strip surface. The texture reveals a slightly inclined weak orientation fiber close to {001}<uvw> [8,9,11,24]. It must be noted though that the HR-EBSD data set presented in Figure 4 does not reveal a statistical texture analysis. Previous work on thin strip steel textures that was conducted using x-ray Bragg diffraction methods [6-12,24] had shown before the occurrence of a weak {001}<uvw> fiber texture. The deviation from an exact {001}<uvw> fiber texture can be attributed to the shape inclination of the grains. The

EBSD data also reveal, as qualitatively observed already in Figure 3, that the region close to the surface of the as-cast material reveals smaller grains than the regions below, indicating growth selection. Also, differences in the ratio between the δ and the γ phase content and in the dispersion of the δ phase between the surface and center layer regions may play a role for the observed differences in the crystal size and morphology.
The image in the middle of Figure 4 reveals the distribution of the two main phases, namely of the γ austenitic face centered cubic (FCC) majority phase and the finely dispersed body centered cubic (BCC) δ minority phase. The image on the right hand side of Figure 4 shows the distribution of the grain boundary character in the same metallographic section. The figure elucidates that most of the interfaces are high angle grain boundaries.

Microstructure after in-line hot rolling and recrystallization annealing

The investigation of the in-line hot deformation parameters imposed after casting is essential for the optimization of the microstructure and the resulting mechanical properties of the final strip. Figure 5 shows the microstructure as obtained from HR-EBSD measurements, taken in longitudinal sections, for three different in-line hot rolling strategies. The three micrographs show the grain structure observed for three different hot rolling variants. The image at the bottom below these three microstructures shows a magnified part of the grain structure of the sample on the right hand side.

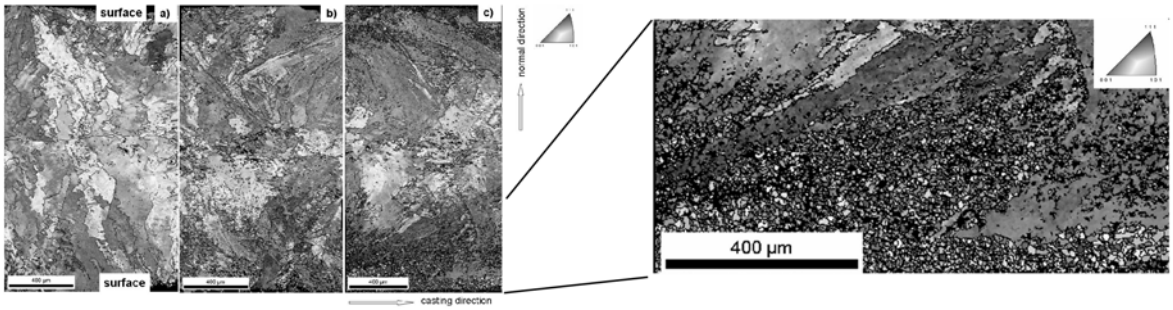

Figure 5. Microstructure mapping obtained from HR-EBSD measurements (longitudinal sections) for three different in-line hot rolling strategies. The bottom figure is a magnification revealing recrystallization. The gray scale code indicates the crystallographic direction which is parallel to the surface in terms of Miller indices {hkl}.

All hot rolling processes were conducted on an industrial in-line mill, Figure 1. Figure 5a on the left hand side shows a microstructure with only weak shape changes of the grains after hot rolling. Recrystallization cannot be observed. The micrograph in the middle (Figure 5b) shows larger shape distortions of the grains. Close to the bottom of the micrograph some recrystallization can be observed. The micrograph on the right hand side (Figure 5c) also shows distorted grain shapes which indicate strong shear deformation particularly close to the surface. It is important to note that this sample reveals a larger volume fraction of finely recrystallized material particularly close to the surface portion where the accumulated plastic strain is usually larger than in the center regions. Figure 6 shows the microstructure of three mappings obtained from HR-EBSD measurements (longitudinal sections). The micrograph on the left hand side is a conventionally produced hot strip. The other two micrographs show microstructures obtained form two different in-line hot rolled strips after final recrystallization treatment. The EBSD maps show a fine and homogeneously distributed grain size for the two heat treated thin cast and in-line rolled strips. The strip cast material is characterized by a very homogeneous microstructure through the strip thickness which suggests that the mechanical properties show only small scatter. Conventionally cast and subsequently hot rolled specimens, in contrast, typically reveal stronger microstructure gradients between the near-surface and the center layer regions owing to the large shears imposed during conventional hot rolling [15-19,24]. Also, the crystallographic

textures are similar in the near surface and center layer regions for the thin cast strips. This fact also indicates a relatively homogeneous deformation history when compared to conventionally hot rolled material.

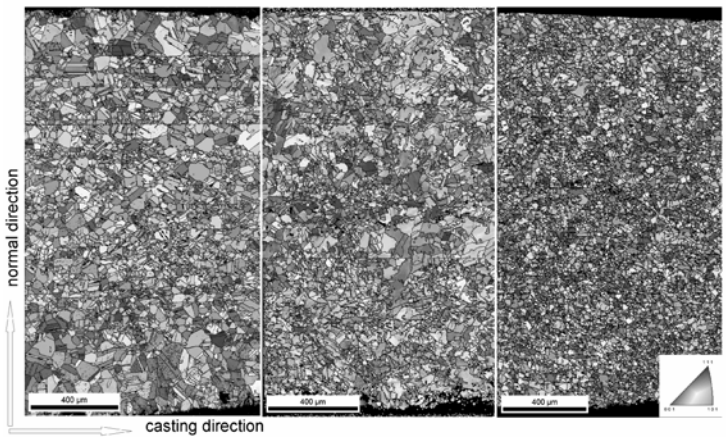

Figure 6. Microstructure mapping and grain size distribution obtained from HR-EBSD measurements (longitudinal sections) for a 304 sample produced via the conventional hot strip route (left) and two 304 thin strip samples after different in-line hot rolling and subsequent recrystallization treatment (middle and right). The gray scale code indicates the crystallographic direction which is parallel to the surface in terms of Miller indices {hkl}.

Mechanical properties of cast, hot rolled, and recrystallized strips

Figure 7 shows the mechanical properties of two samples of a thin strip cast, hot rolled, and recrystallized strip. Two samples from different positions were taken to probe the heterogeneity of the as-cast material. It was in some cases observed that the α‘ and δ-phases were not homogeneously distributed between the center and the surface. The EBSD maps show the distribution of the δ-phase (bright) plus the deformation-induced α‘ martensite (bright) and of the austentite (dark) for the two samples. The δ-phase has BCC crystal structure and the strain-induced α‘ martensite has slightly tetragonal near BCC structure. This means that both phases can be differentiated from the FCC austenite. The volume increase of α‘ martensite upon plastic straining is a known phenomenon in these steels which is related to the low thermodynamic stability of the austenitic phase [8]. Deformation also leads to a very small volume fraction of the deformation-induced hexagonal ε phase, but the α‘ martensite is generally the dominant deformation-induced phase. Depending on the thermodynamic and microstructure details such as the Cr/Ni equivalent ratio and the grain size, up to 45vol.% α‘ martensite can be formed. The exact location, arrangement and volume fraction of the α‘ martensite is of relevance for the forming properties. Among the different methods to quantify α‘ (magnetic, metallography, hardness, EBSD) the EBSD method is considered the most reliable one. The mechanical properties presented in Figure 7 are comparable to those obtained for samples that are manufactured via the conventional continuous casting and hot rolling route.

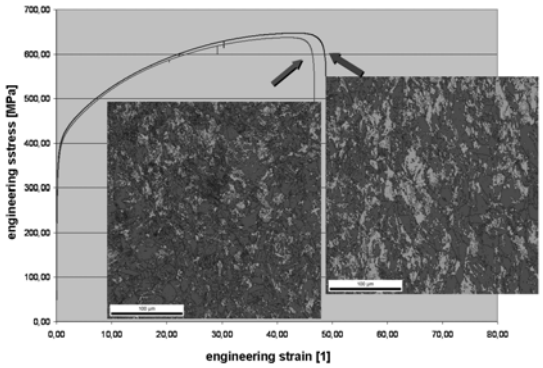

Figure 7. Stress-strain curves of two samples of a thin strip cast, hot rolled, and recrystallized strip. Two samples from different regions were taken to probe the homogeneity of the material. The EBSD maps show the corresponding distribution of the delta-phase plus the deformation-induced α‘ martensite (bright) and of the austentite (dark) for the two samples.

Conclusions

We presented recent advances in the optimization of the microstructure and properties of thin strip cast austenitic (AISI 304, 1.4301) stainless steel. The main conclusions are:

- Austenitic 304 stainless steels in the hot rolled, annealed and pickled condition can be produced by thin strip casting with equivalent mechanical properties and even better microstructure homogeneity than steels produced by the conventional continuous casting processing route.
- The formation of deformation-induced α‘ martensite in austenitic stainless steels produced by the thin strip casting route is similar as in conventionally produced 304 steels.
- Precise characterization of the different phases, interfaces, and crystallographic textures can be conducted by using a high resolution EBSD method.

References

[1] M. Walter, G. Stebner, J.M. Damasse, P. Tolve, G. Hohenbichler, Continuous Casting Conference 2000, Linz, Austria, June 2000
[2] U. Albrecht-Früh, R. Degenhardt, G. Porcu, L. Pöcksteiner, J.M. Damasse, C. Marchionni, International ATS Steelmaking Days, 14. December 2000, Paris
[3] H.-U. Lindenberg, J. Henrion, K. Schwaha, G. Vespasiani, Stahl Eisen 121 (2001) 97-104
[4] H.-U. Lindenberg, J. Henrion, K. Schwaha and G. Vespasiani, Rev. Met. Paris, N°7-8 (2002), 615-627
[5] H. Legrand, D. Themines, R. Degenhardt, U. Albrecht-Früh, C. Moellers, A. Flick, Proceedings 4th European Stainless Steel Science and Market Congress, June 10-13, 2002, Paris, France, 1-7
[6] D. Raabe, M. Hölscher, F. Reher, K. Lücke: Scripta Metall. 29 (1993) 113–116
[7] D. Raabe, M. Hölscher, M. Dubke, H. Pfeifer, H. Hanke, K. Lücke: Steel Research 4 (1993) 359–363
[8] D. Raabe: Acta Materialia 45 (1997) 1137–1151
[9] D. Raabe: Materials Science and Technology 11 (1995) 461–468
[10] D. Raabe: Journal of Materials Science 30 (1995) 47–52
[11] D. Raabe: Metall. Mater. Trans A 26A April (1995) 991–998
[12] D. Raabe, H. Krause: Proc. 11th Int. Conf. Textures Materials ICOTOM 11, Sept. 16-20, 1996, Xi’an, China, eds.: Z. Liang, L. Zuo, Y. Chu, Vol. 2, 854–859

[13] D. Raabe, H. Krause, A. D. Rollett, A. Teicher: Proc. of the 12th Inter. Conf. on Textures of Materials ICOTOM 12, Aug. 9–13, 1999, Montreal, eds.: Jerzy A. Szpunar, NRC Research Press, National Research Council of Canada, 1999 (2) 1015–1024
[14] M.-Y. Huh, J.-H. Lee, S. H. Park, O. Engler, D. Raabe, Steel Research 76 (2005) 797-806
[15] D. Raabe, K. Lücke: Materials Science and Technology 9 (1993) 302–312
[16] D. Raabe, K. Lücke: Scripta Metall. 26 (1992) 1221–1226
[17] A. Fedosseev, D. Raabe, Scripta metall. 30 (1994) 1–6
[18] M. Hölscher, D. Raabe, K. Lücke, Acta metall. 42 (1994) 879–886
[19] M. Hölscher, D. Raabe, K. Lücke, Steel Research 62 (1991) 567–575
[20] I. Thomas, S. Zaefferer, F. Friedel, D. Raabe, Adv. Eng. Mater., 2003, 5, 566-570
[21] A. Bastos, S. Zaefferer, D. Raabe, C. Schuh, Acta Mater. 54 (2006) 2451–2462
[22] L. Storojeva, D. Ponge, R. Kaspar and D. Raabe, Acta Mater. Vol. 52 (2004) 2209-2220
[23] R. Song, D. Ponge, R. Kaspar, D. Raabe, Zeitschrift für Metallkunde 95 (2004) 513–517
[24] D. Raabe, Steel Research 74 (2003) 327-337

INFLUENCE OF NITROGEN ON THE MECHANICAL BEHAVIOUR OF TYPE 316L SS

V. Ganesan, M.D. Mathew, K. Bhanu Sankara Rao, B. Raj

Indira Gandhi Centre for Atomic Research, India

Abstract

Nitrogen-alloyed 316L stainless steel is used as a structural material for high temperature fast breeder reactor components with a design life of 40 years. With a view to increase the design life to 60 years and beyond, studies are being carried out to develop 316L grade austenitic stainless steels with superior tensile, creep and low cycle fatigue properties. The influence of nitrogen on the creep and tensile behaviour of 316L stainless steel has been studied at nitrogen levels of 0.07, 0.11, 0.14 and 0.22 wt%. Tensile properties were studied at temperatures of 300 K, 523 K, 623 K, 723 K, 823 K, 923 K, 1023 K and 1123 K at a constant strain rate of 3.0×10^{-3} s^{-1}. Yield strength and ultimate tensile strength were found to increase linearly with increase in nitrogen content. Tensile ductility generally showed a decrease with increase in nitrogen content. Creep properties were studied at 923 K at various stress levels. Creep rupture strength increased substantially with increasing nitrogen content, while the steady state creep rate showed a corresponding. Rupture ductility was generally above 40% at all the test conditions and nitrogen contents.

Introduction

For high temperature structural components of sodium cooled fast reactors, 316L(N) stainless steel (SS) containing 0.02-0.03 wt% carbon and 0.06-0.08 wt% nitrogen has been selected. By keeping the carbon content low, the susceptibility to sensitization of the heat affected zone (HAZ) in welded components can be minimized and thus the potential for stress corrosion cracking of HAZ in a corrosive environment, can be alleviated. Alloying with 0.06-0.08 wt% nitrogen helps to increase the high temperature strength of 316L SS to levels comparable to that of 316 SS. In order to increase the economic competitiveness of fast reactors, there is a strong desire to increase the design life time from the current level of 40 years to at least 60 years. As part of the effort to develop structural materials suitable for longer design life, the influence of nitrogen at concentrations higher than 0.08 wt% on the high temperature mechanical properties of type 316L SS are being evaluated. Nitrogen has been shown to improve creep and fatigue strength at high temperatures and fracture toughness at cryogenic temperatures in ferritic steels, austenitic steels, martensitic steels and duplex steels[1,2].

Four heats of 316L SS, containing 0.07, 0.11, 0.14 and 0.22 wt% nitrogen (designated as 316LN SS) were produced to study the effect of nitrogen on the tensile and creep properties of 316 L SS. The carbon content in these heats was maintained at ~ 0.03 wt. % and the actual chemical composition of all other elements was similar (Table 1). The aim of this investigation is to optimize the nitrogen content of the steel in order to obtain optimum combination of tensile, creep and low cycle fatigue properties. This paper presents the results on the influence of

nitrogen on the high temperature tensile and creep properties. Although there are several studies on the influence of nitrogen on mechanical properties of steels[3], there have been no systematic studies on the influence of nitrogen on the mechanical properties of 316L SS over such a wide range.

Experimental

Four heats of 316LN SS were produced through double melting process. Primary melting of the steel was carried out by an air induction melting. The charge consisted of pure raw materials in order to achieve good control on the chemical composition of the steel. During primary melting, nitrided ferrochrome was used to achieve the required amounts of nitrogen in the different heats. Other major and minor elements were controlled to the same level in all the heats. Secondary melting was carried out by electro slag refining process in order to produce the steel with very low inclusion content. The ESR ingots were hot forged into slabs and subsequently hot rolled into plates of 22 mm thickness and finally given a solution annealing treatment between 1323 and 1423 K. Equiaxed grains free of carbide precipitates were observed in all the heats. The grain size of the four heats varied in a small range of 78 to 96 μm. The chemical composition of the four heats of 316LN SS and their grain sizes are given in Table 1. Tensile studies were carried out at 300 K, 523 K, 623 K, 723 K, 823 K, 923 K, 1023 K and 1123 K at a constant strain rate of $3.0 \times 10^{-3}\ s^{-1}$. Creep tests were carried out at 923 K at different stress levels in the range 140-225 MPa.

Table 1. Chemical Composition of 316LN SS [wt%].

Designation	N	C	Mn	Cr	Mo	Ni	Si	S	P	Fe
7N	0.07	0.027	1.7	17.53	2.49	12.2	0.22	0.0055	0.013	Bal.
11N	0.11	0.033	1.78	17.62	2.51	12.27	0.21	0.0055	0.015	Bal.
14N	0.14	0.025	1.74	17.57	2.53	12.15	0.20	0.0041	0.017	Bal.
22N	0.22	0.028	1.70	17.57	2.54	12.36	0.20	0.0055	0.018	Bal.

Results

Tensile Properties

The variation of yield strength (YS) and ultimate tensile strength (UTS) with nitrogen content at different test temperatures is shown in Figs. 1(a) and 1(b) respectively. Yield strength and ultimate tensile strength increased linearly with increase in nitrogen content between 0.07 and 0.22 wt% at all the test temperatures. Based on the data shown in Figs. 1(a) and 1(b), master equations have been developed to predict YS and UTS as a function of nitrogen content (N) and tensile test temperature (T). The predicted equations are given below:

$$YS = 246 + 1133N - 0.17T - 1.71NT + 9.5\times10^{-4}NT^2 \qquad (1)$$

$$UTS = 925 + 1334N - 2.2T - 2.5NT + 0.003T^2 + 0.0037NT^2 - 1.7\times10^{-6}T^3 - 1.9\times10^{-6}NT^3 \qquad (2)$$

Figures 2 (a) and 2(b) show a comparison between predicted and experimental YS and UTS values. The entire range of predicted data falls within 95% confidence interval of the experimental data.

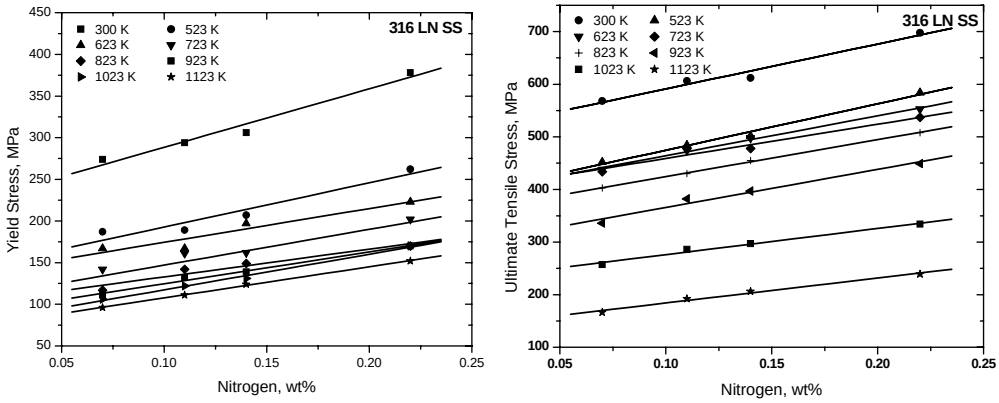

(a) (b)

Figure 1. Influence of nitrogen content and test temperature on (a) yield strength and (b) ultimate tensile strength.

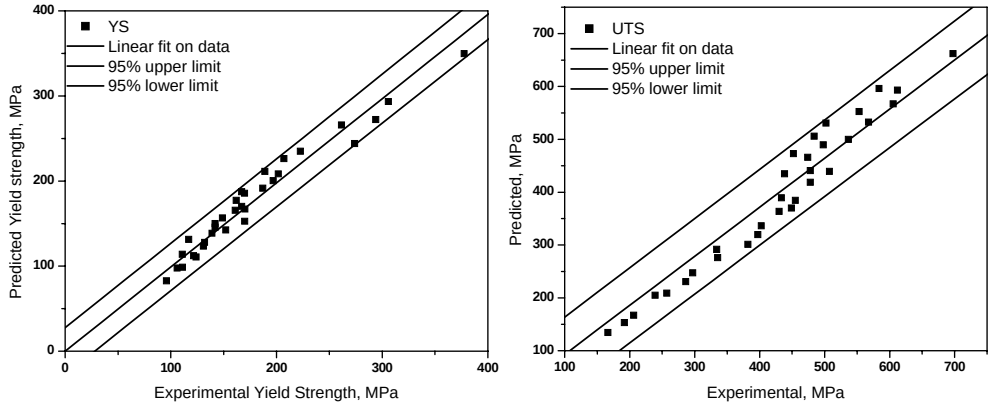

(a) (b)

Figure 2. Comparison between predicted values and experimental data for (a) yield strength and (b) ultimate tensile strength.

The beneficial effects of nitrogen observed in this study on yield and ultimate tensile strength are in agreement with the results of Kim et. al.[4], who showed that nitrogen increases yield and ultimate tensile strength in 316L SS containing 0.02 wt% carbon, and nitrogen varying between 0.01 and 0.15 wt%. Mullner et al.[5] have also reported beneficial effect of nitrogen on the tensile properties of 316L SS.

The variations of uniform and total elongation with nitrogen content at various test temperatures are shown in Figs. 3(a) and 3(b) respectively. Two different trends can be observed from these figures; one for the high temperature range 823-1123 K and the other for the lower temperature range of 300-723 K. Uniform and total elongation showed a minimum between 0.10 and 0.15 wt% nitrogen in the range 300-723 K. On the contrary, a gradual decrease in ductility was observed between 0.10 and 0.15 wt% nitrogen in the range 823-1123 K. Beyond 0.15 wt%, ductility did not show any significant change with nitrogen content. The total elongation varied in the range of 41 to 57 % at room temperature, and in the range of 33 to 69 % at 1123 K.

316 LN SS exhibited dynamic strain ageing (DSA) behaviour at intermediate temperatures. In the heat containing 0.07 % nitrogen, serrations were observed in the load-elongation curves between 723 and 923 K. The temperature window of serrated flow narrowed as the nitrogen

content increased from 0.11 to 0.22 wt.%; in the heat containing 0.22 wt. % of nitrogen, serrated flow was observed only at 923 K. The tensile tests were carried out at a strain rate of $3x10^{-3}$ s^{-1}.

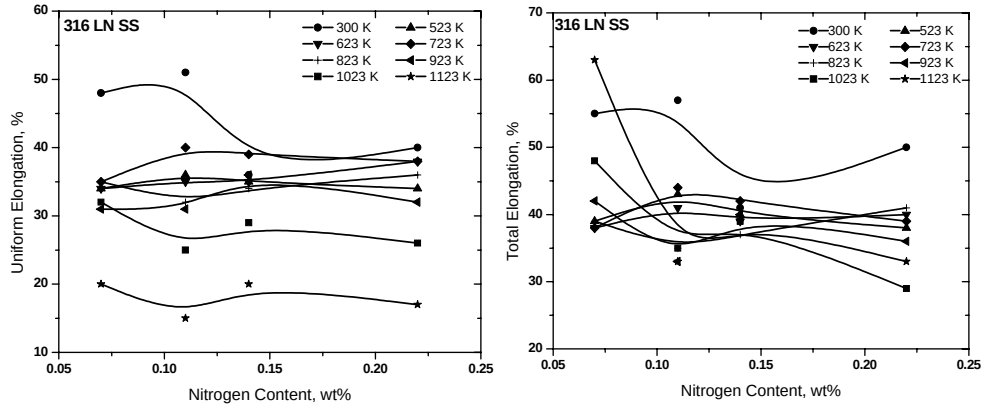

Figure 3. Influence of nitrogen and test temperature on (a) uniform elongation and (b) total elongation

Creep Properties

Creep tests have been carried out at 923 K at stress levels of 140, 175, 200 and 225 MPa. The rupture lives varied in the range of 50 to 4400 hours. Low stress tests are currently in progress. Figure 4(a) shows the influence of nitrogen on the creep strain-time curves at 175 MPa. Creep strain accumulation depended on the nitrogen content. The variation of steady state creep rate with stress showed a power law relationship for all the nitrogen contents (Figure 4(b)). The power law exponent varied between 6.4 and 13.7 depending upon the nitrogen content. Figure 5(a) shows the variation of rupture life with nitrogen content at various stress levels. Significant increase in rupture life was observed with increase in nitrogen content at all the stress levels. Rupture life increased almost 10 times by increasing nitrogen content from 0.07 wt% to 0.22 wt%. On the other hand, rupture ductility decreased with increase in nitrogen content as shown in Figure 5(b). Rupture ductility tends to increase with increase in rupture life although a minimum in ductility was observed at short durations of the order of a few hundreds of hours.

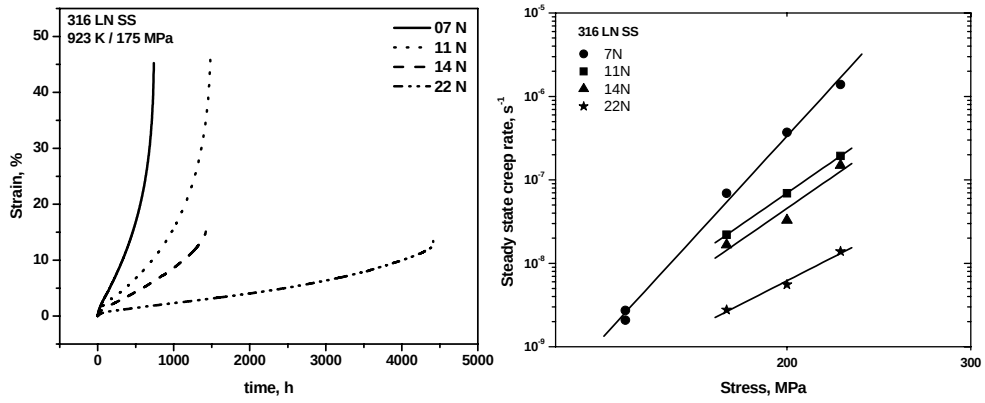

Figure 4. Influence of nitrogen content on (a) creep curve at 225 MPa and (b) steady state creep rate at various stress levels.

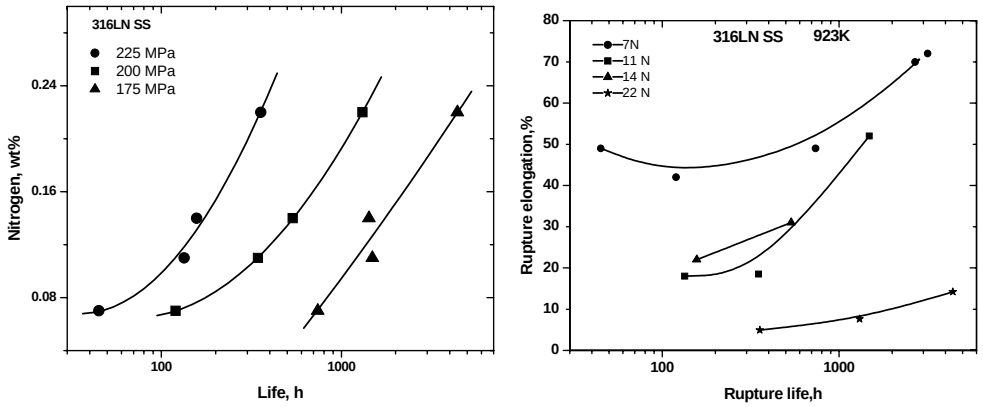

(a) (b)

Figure 5. Influence of nitrogen content on (a) rupture life and (b) rupture elongation.

Discussion

Nitrogen is generally considered as a good solid solution strengthening element and thus improves tensile, creep and fatigue strength of austenitic stainless steels[6-13]. Besides solid solution hardening, nitrogen also causes decrease in stacking fault energy, precipitation strengthening, clustering and order strengthening depending upon the amount of nitrogen in the steel and also the time-temperature conditions. Nitrogen dissolved in austenitic steels causes higher dilation and therefore a strong pinning of nitrogen by dislocations. Compared to carbon, the effective binding energy between nitrogen atoms and dislocations is increased with the nitrogen content in austenitic steel, whereas such dependence is not significant for carbon. Nitrogen interacts with substitutional (s) elements also, and tends to form interstitial-substitutional (i-s) atomic complexes[14].

An empirical relationship between room temperature yield strength, nitrogen content and grain size has been earlier reported by Degallaix et al.[7] for a niobium and vanadium bearing austenitic SS containing up to 0.39 wt% nitrogen. The strengthening effect has been attributed to lowering of stacking fault energy of the system by nitrogen addition. Liu et al.[15] studied the tensile properties of 316L SS and 316L(N) SS containing 0.14 wt% nitrogen. 316L(N) SS showed increase in tensile strength as compared to 316L SS and this was attributed to solid solution strengthening by nitrogen. The effect of nitrogen in the range of 0.10 to 0.37 wt% on tensile properties of a duplex stainless steel was studied by Park and Lee[16]. It was shown that ultimate tensile strength and ductility increased but yield strength decreased slightly with increasing nitrogen content. These variations were explained in terms of the different amounts of ferrite and austenite phases in the duplex stainless steel at different nitrogen contents. Matsuo et al.[17] studied the effect of nitrogen between 0.01 and 0.2 wt% and carbon in the range of 0.03 to 0.07 wt% on the creep properties of Fe-25Cr-20Ni SS in the temperature range of 973 to 1273 K. Minimum creep rate was found to decrease with increase in nitrogen concentration. The solid solution strengthening effect was found to be effective even at 1273 K and was independent of the carbon concentration. Studies carried out by Nakazawa et al.[18] in modified 316 SS containing nitrogen in the range of 0.02 to 0.12 wt% and carbon in the range of 0.013 to 0.049 wt% showed that nitrogen increases rupture strength without decreasing ductility. Our studies have shown that whereas nitrogen decrease minimum creep rate and increases rupture strength very significantly, creep rupture ductility decreases with increasing nitrogen content.

Conclusion

Yield strength and ultimate tensile strength of 316L stainless steel increased significantly by alloying with nitrogen in the range of 0.07 to 0.22 wt%. The improvement in strength was observed at all test temperatures between 300 and 1123 K. Equations have been proposed to predict yield strength and ultimate tensile strength as a function of nitrogen content and test temperature. Dynamic strain ageing was observed over a limited range of temperatures. The range of DSA temperature decreased with increasing nitrogen content. With increasing nitrogen content, significant increase in creep rupture life, decrease in steady state creep rate and decrease in creep rupture ductility were observed.

Acknowledgement

The authors thank Dr. P.R. Vasudeva Rao, Director, Metallurgy and Materials Group, IGCAR for his support and keen interest in this work.

References

1. V.G. Gavriljuk and H. Berns, 'High Nitrogen Steels', 135; 1999, New York, Springer-Verlag Berlin Heidelberg.
2. J.R. Kearns in R.A. Lula, 'Proceedings of Conference on New Developments in Stainless Steel Technology', 117; 1985, ASM, Metals Park, OH.
3. C.R. Brinkman, *J. Pressure Vessel Technology*., 2001, 123, 75.
4. D.W. Kim, J. Mater. Sci., 1998, 33, 675.
5. P. Mullner, C. Solentaheler, P. Uggowitzer and M.O. Spiedel, Mater. Sci. Engg., 1993, A164, 164.
6. Mechanical Behaviour of Nitrogen-bearing Steels - M.D. Mathew and V.S. Srinivasan in *Monograph on High Nitrogen Austenitic Steels and Stainless Steels*, U. Kamachi Mudali and Baldev Raj (Eds.), Narosa Publications, New Delhi, 2004, pp.182-204.
7. S. Degallix, J. Foct and A. Hendry, Mater. Sci. Tech., 1986, 2, 946.
8. M.D. Mathew, S. Latha and K.B.S. Rao, Mater. Sci. Engg , 2007, 456, 28-34.
9. M.D. Mathew, S. Latha, K.B.S. Rao and S.L.Mannan, Transactions of The Indian Institute of Metals, 2005, 58, 269-273.
10. G. Sasikala, M.D. Mathew, K.B.S. Rao and S.L. Mannan, Metallugical Transactions A, 2000, 31A, 1175-1186.
11. G. Sasikala, M.D. Mathew, K.B.S. Rao and S.L. Mannan, Journal of Nuclear Materials, 1999, 273, 257-264.
12. M.D. Mathew, G. Sasikala, K.B.S. Rao and S.L. Mannan, Materials Science and Engineering, 1991, A148, 253.
13. V.S. Srinivasan, M. Valsan, K.B.S. Rao, S.L. Mannan and B. Raj, International Journal of Fatigue, *2003*, 25, 1327-1338.
14. M.L.G. Byrnes, M. Grujici and W.S. Owen, Acta Met., 1987, 35, 1853.
15. F. Liu, J.G. Jung and S.W. Nam, Key Engineering Materials, 2007, 345-346, 69-72.
16. Y-H. Park and Z-H. Lee, Mater. Sci. Engg., 2001, A297, 78-84.
17. T. Matsuo, N. Morioka, S. Kaise, M. Kikuchi and R. Tanaka, Effect of nitrogen on creep deformation of 25Cr-28Ni austenitic steels - solid solution strengthening due to nitrogen, in J. Foct and A. Hendry (eds.), HNS 88, Lille, France. May 1988, The Institute of Metals, London, 1989, p. 213.
18. T. Nakazawa. H. Abo, M. Tanino, H. Komatsu, T. Nishida and M. Tashimo, Effects of nitrogen and carbon on creep properties of type 316 SS, in J. Foct and A. Hendry (eds.), *HNS 88, Lille, France, May* 1988, The Institute of Metals, London, 1989, pp. 218-224.

BAKE HARDENING OF SOME AUSTENITIC STAINLESS STEELS

R. Ruoppa, T. Taulavuori

Tornio Research Centre, Outokumpu Tornio Works, Finland

Abstract

The influence of cold rolling reduction and bake hardening on the properties of some austenitic stainless steels were studied. The wide range of steel grades studied was EN 1.4301 (AISI 304), EN 1.4310 (AISI 301), EN 1.4318 (AISI 301LN), EN 1.4372 (AISI 201), "201 Cu" and "204 Cu". The steels were cold rolled in the laboratory scale rolling mill to the thickness reduction of 10 %, 20 % and 30 %, respectively. Additionally the steels were annealed 20 minutes at the temperature of 170°C. The steels were mechanically tested by tensile test in both rolling direction and transverse to the rolling direction. The α'-martensite content of the steels after cold rolling and ageing was measured, too. Formability was tested by the Erichsen test.

The results showed that the bake hardening tempering had an influence on the mechanical properties of the steels. The yield strength increased by the influence of strain ageing with all the steels studied. The maximum increase in the strength was in the level of 230 N/mm^2 depending on the degree of cold working prior to the ageing and the steel grade. Aging also affected on the anisotropy between rolling and transverse direction caused by the cold working. Despite the increase of the strength, the elongation and formability were maintained. It can be concluded that the strength of strain hardened austenitic stainless steels can be improved remarkably by bake hardening without a loss in the ductility and formability properties.

Introduction

Strain ageing is well known in body-centered cubic metals. In deformed material, yield point reappears after some period of time and the material is strengthened and hardened.[1] In iron, strain ageing is slow at room temperature but in 200°C a strong yield point returns after ageing only a few seconds.[2] This phenomenon is associated on the diffusion of interstitial atoms C and N, which are locking dislocations by forming atmospheres around them.[1, 2] This mechanism is most closely associated with iron and low-carbon steels.

Strain ageing has also been observed in face-centered cubic (fcc) structure, but the mechanism obviously differs from the mechanism in body-centered cubic (bcc) structure. In bcc metals, the interstitial atoms form an asymmetric stress field to the surrounding matrix, which makes them capable to react with all dislocations. In fcc metals, the interstitial atoms form spherically symmetric stress fields around them, which prevents the single interstitial atoms to lock dislocations.[3] However, strain ageing in fcc metals has been suggested to take place by the formation of pairs between interstitial atoms, substituting atoms and interstitial atoms, interstitial atoms and vacancies. These pairs create stress fields, which are strong enough to react with the stress fields of dislocations.[3]
Austenitic stainless steels can be strengthened by cold working due to the deformation induced martensite ($\gamma \rightarrow \alpha'$). It has been reported that ageing of cold worked austenitic stainless steel can

result in further increase in strength by the strain ageing.[4-11] Sandström and Bergqvist[8] assumed that the hardening of N alloyed stainless steel due to the strain ageing is related to the pairing of Cr and N atoms. Rathbun et al.[4] concluded that the increase in strength is associated with the strengthening of the martensite phase and no ageing occurs in the deformed austenite phase. They suggested that the active mechanism is associated with short-range redistribution of C atoms to dislocations. Talonen et al.[9] studied strain aging of steel grades 1.4301 and 1.4318 and concluded that the ageing process is related to the tempering of strain-induced α'-martensite, which involves the redistribution of the N and C atoms, and thus, cause an increase in yield strength. Changes in the residual micro-stress state were assumed to affect the ageing behaviour.

The aim of this study was to find out the effect of strain ageing on the mechanical properties of several austenitic stainless steels by a heat treatment in relatively low temperature similar to the bake hardening treatment performed on formed automotive components. The austenitic stainless steels studied had different chemical compositions and the tendency to form martensite in cold working.

Experimental procedure

The steels chosen for this study were cold rolled and annealed in mill scale at Outokumpu Tornio Works. Three of them were CrNi steels EN 1.4301 (AISI 304), EN 1.4310 (AISI 301) and EN 1.4318 (AISI 301LN). Other three were CrMn steels having internal Outokumpu designation 704 (EN 1.4372 and AISI 201), 705 ("201 Cu") and 703 ("204 Cu") with varying low Ni content. The chemical composition, Md_{30} temperature after Nohara-equation[13] and thickness of each steel are listed in Table 1.

Table 1. Compositions in weight percent, initial sample thickness and Md30-temperature calculated after Nohara equation of the experimental stainless steels

Material	Thickness (mm)	C	Si	Mn	P	S	Cr	Ni	Mo	Cu	N	Md_{30} (°C)
EN 1.4301	0.80	0.055	0.49	1.70	0.030	0.001	18.3	8.1	0.17	0.39	0.050	-16.9
EN 1.4310	1.27	0.100	1.11	1.24	0.024	0.001	16.7	6.3	0.66	0.25	0.078	15.7
EN 1.4318	1.19	0.022	0.43	1.26	0.028	0.001	17.4	6.5	0.21	0.22	0.127	27.5
703	1,01	0,079	0,40	9,00	0,032	0,004	15,2	1,1	0,03	1,68	0,115	95,2
704	1,01	0,061	0,32	7,05	0,032	0,003	16,9	4,4	0,13	0,25	0,182	9,4
705	1,01	0,047	0,29	5,70	0,028	0,002	17,3	4,7	0,21	2,39	0,107	-17,9

Prior to tensile and ageing tests, the steels were cold rolled in a laboratory scale cold rolling mill to the thickness reduction of 10%, 20% and 30%, respectively. Bake hardening was performed in air furnace for the steels cold rolled 20% and 30%. The annealing time was 20 minutes and the temperature was 170°C. The α'-martensite content was measured with Fischer Feritscope MP30 equipment. The Feritscope readings were converted to α'-martensite contents by paying attention to thickness of the sample based on the manufacturer data and multiplying with the factor of 1.7 based on Talonen et al. [12] study. The tensile tests were carried out both in the rolling direction (RD) and transverse to the rolling direction (TD) using constant strain rate of 0,003 1/s. The formability of the steels was tested with Erichsen cup tests.

Results and discussion

The contents of the α'-martensite measured from each steels after cold rolling into the reduction of 0…30 % and aging 20 min at 170°C (cold rolling reduction 20 % and 30 %) are shown in Figure 1 a.

The α'-martensite content was increasing with increasing cold rolling reduction. Increase in the α'-martensite content was strongest on grade 1.4318, 1.4310 and 703, having Md_{30} temperatures +27°C, +17°C and +95°C, respectively. The grades 1.4301, 704 and 705, were less pronounced to α'-martensite formation, which may be anticipated their lower Md_{30} temperatures. However, it is obvious, that Nohara equation seems not to be valid with the CrMn steels because the Md_{30} values seem to be too high compared to the α'-martensite content. Ageing at 170°C had negligible effect on the amount of the α'-martensite.

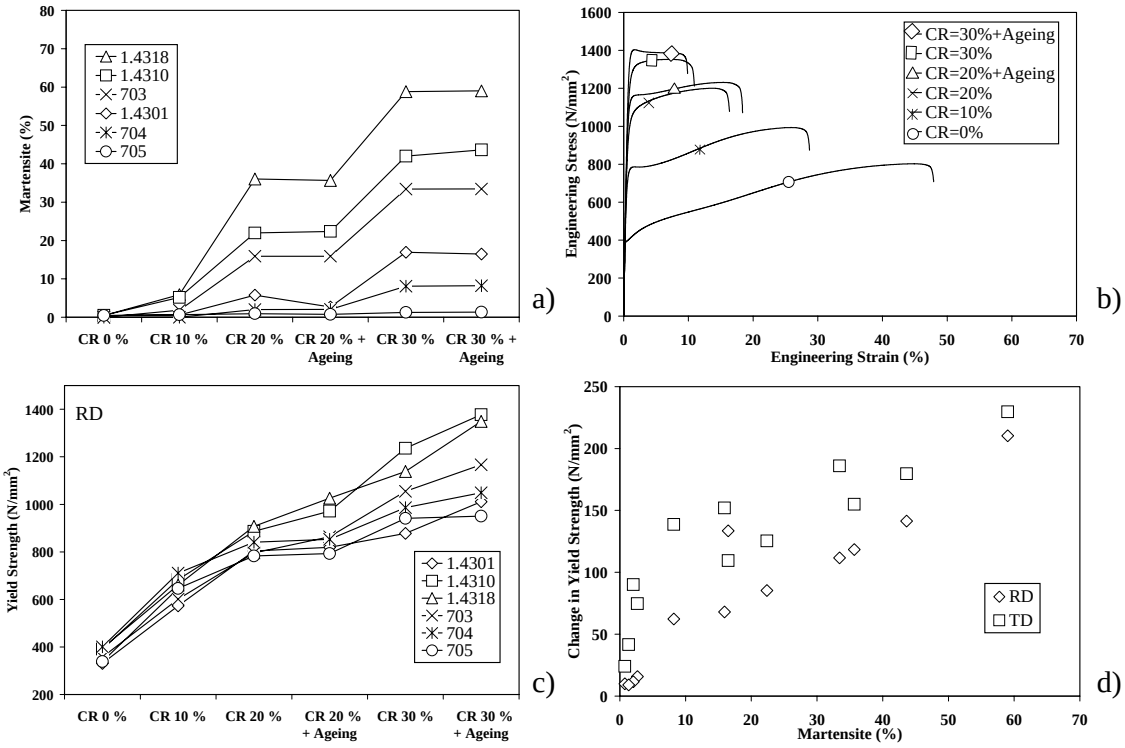

Figure 1. Effect of cold rolling reduction and ageing at 170°C on a) α'-martensite content, b) tensile curves for the grade 1.4318 and c) yield strength, d) Relationship between α'-martensite content and change in yield strength after ageing for the studied grades

Stress-strain curves of the cold rolled grade 1.4318 before and after ageing are shown in Figure 1 b. Flow stresses are increasing with increasing cold rolling reduction, but the ageing is also increasing the flow stresses. Both the yield strength and the ultimate tensile strength are increasing. The effect of cold rolling reduction and ageing treatment on the yield strengths of all the studied steels are shown in Figure 1 c. Strengthening of grades 1.4318, 1.4310 and 703 was most pronounced. It can be concluded that the ageing treatment improved the yield strength of all the steels studied as seen in Figure 1 d. The efficiency of the ageing is increasing with increasing α'-martensite content, which supports the assumption, that the strain ageing phenomenon is related to the presence of α'-martensite phase induced by the cold working like it was concluded in previous studies.

However, also on grades 1.4301 and 704 and 705, which did not have more than about 1…5 % α'-martensite after 20% cold working, the yield strength after ageing increased 10…90 N/mm^2. This indicates that in addition to the α'-martensite phase, strengthening may also occur in the austenite phase. The mechanism is possibly related to the pairing of e.g. interstitial atoms and their interaction with dislocations like it was earlier described with the ageing in fcc metals.

The changes in the yield strengths of the studied steels after various cold rolling reductions and ageing 20 min at 170°C are summarized in Figure 2 a and 2 b. It can be seen seen that the effect of the strain ageing was most proneunced in the grade 1.4318. The yield strength increased 118…230 N/mm^2 depending on the cold rolling reduction.

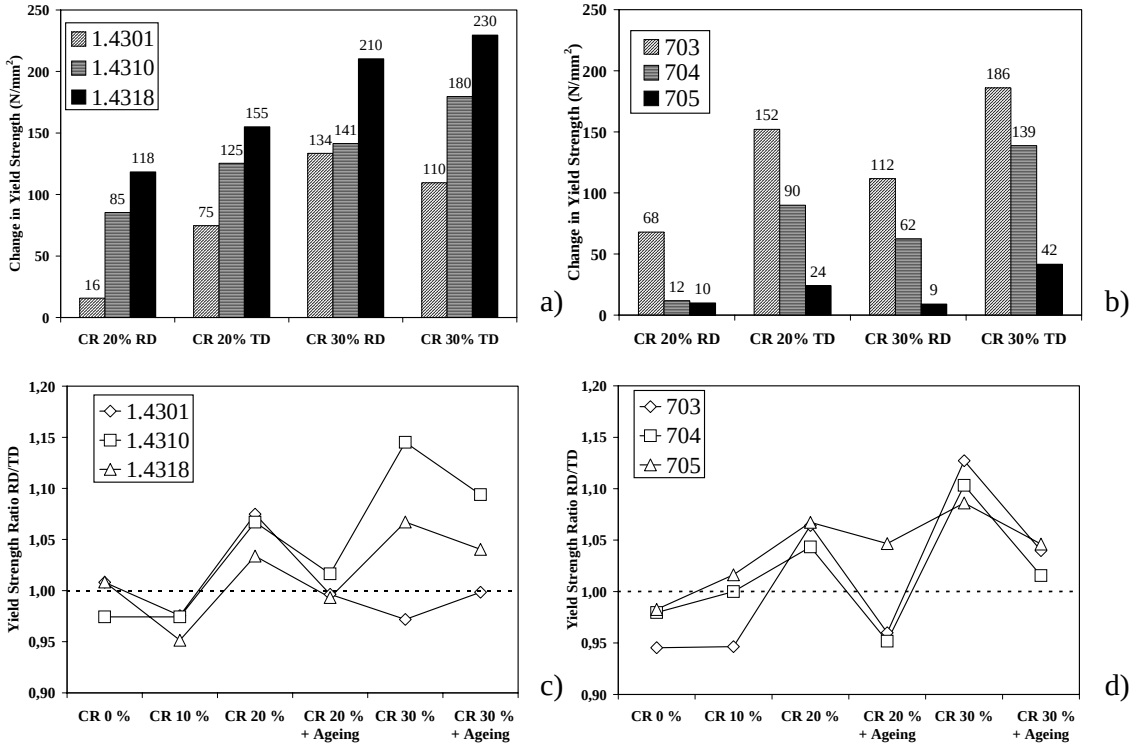

Figure 2. a) and b): change in the yield strength of 20 % and 30 % cold rolled steels in parallel to rolling direction and transverse to rolling direction after aged at 170°C, c) and d): effect of cold rolling reduction and ageing at 170°C on the ratio of yield strength measured in parallel to rolling direction and transverse to rolling direction

The anisotropy of the yield strength values measured transverse to the rolling direction and parallel to the rolling direction, which pronounced when the degree of cold working increases. In Figure 2 c and 2 d the ratio of the yield strength in rolling direction and in transverse direction RD/TD is illustrated. When cold rolling reduction of the CrNi steels reached 20 %, the ratio was 1,03…1,07 but when the steels were additionally aged at 170°C, the ratio decreased close to 1, which means that yield strengths are nearly equal in both directions. It is obvious that the ageing has an influence on the anisotropy of the yield strength caused by the cold working and may reduce it in most cases.

The influence of the cold working and the ageing on formability of the steels was also evaluated. The fracture elongations of the steels are shown in Figure 3 a and 3 b. It can be clearly seen that the elongation values were decreasing with increasing cold rolling reduction. The best yield strength – elongation combination achieved was 1377 N/mm^2 – 13 % for the grade 1.4310 with 42 % α'-martensite content after 30 % cold rolling and and ageing. Respectively, for the low carbon grade 1.4318 with α'-martensite content of 59 %, equal yield strength was reached, but the elongation was decreased after ageing.

In most cases elongations stayed at the same level as they were before the ageing although yield strengths increased. Thus, it could be assumed that stretch-formability of the steels was not impaired due to the ageing. Stretch-formability was tested with Erichsen cup test and the results

are shown in Figure 3 c and 3 d. It can be seen that the Erichsen indexes decreased with increasing cold working reduction. However, after the ageing, Erichsen indexes even slightly increased. This means that the stress-formability of the steels was not impaired due to the ageing. These results and the measured fracture elongations before and after ageing are supporting each other.

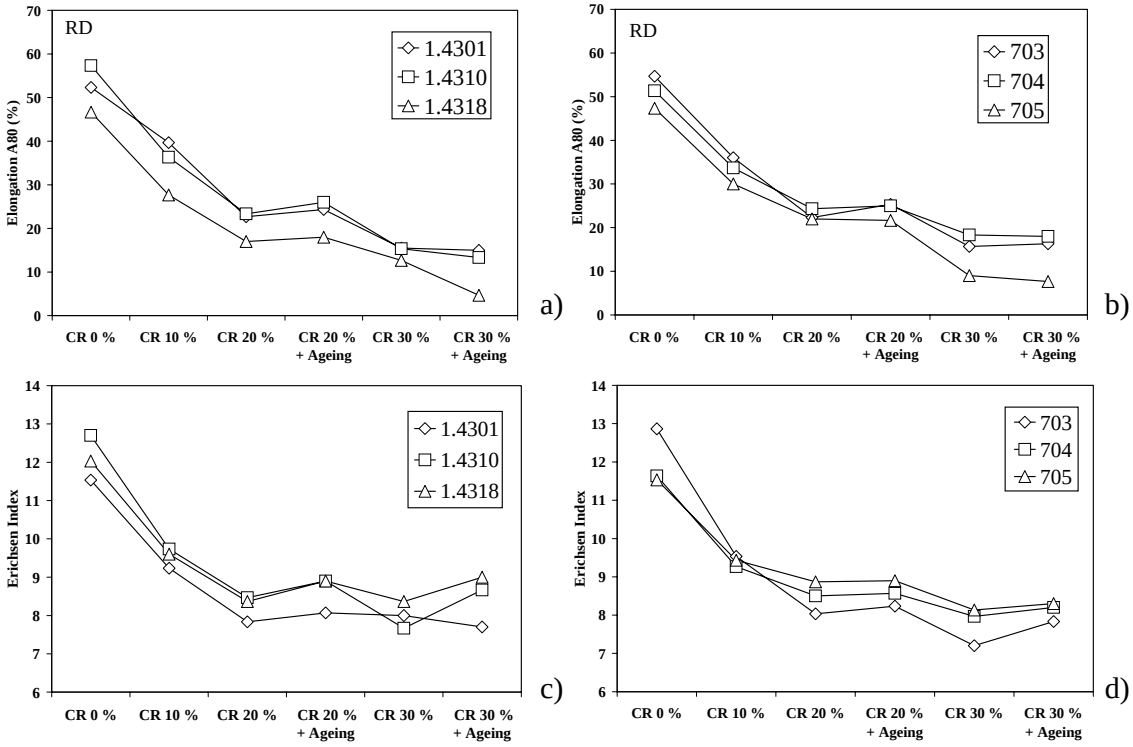

Figure 3. The effect of cold rolling reduction and ageing treatment at 170°C on a) and b): A80 elongation of the steels. Elongation to fracture was measured in parallel to rolling direction, c) and d): stretch-formability of the steels evaluated with Erichsen Index

Knowing the result that the ductility of the steels is not impaired despite the increase in the strength the mechanism of the ageing may also be considered. Strengthening of austenite phase can be assumed to decrease ductility so that the ductility of the α'-martensite phase should be increasing respectively for maintaining overall ductility of the steel. This is possible if the α'-martensite phase is tempered with increasing ductility at the same time with strengthening of the austenite phase. This explanation may seem quite reasonable.

Conclusions

Results showed that all the steels studied are exhibiting strain ageing phenomenon. The yield strength increase is resulted after a cold deformation and the further formation of strain-induced martensite. Additionally aging treatment at relatively low temperature e.g. 20 min at 170°C improves the mechanical properties of the studied steel grades. This ageing treatment corresponds to the bake hardening treatment on formed automotive components.

Increase in the yield strength correlates with the α'-martensite fraction. However, the strength was increased after ageing with very low α'-martensite content. It may be concluded that the mechanism of ageing in deformed austenitic stainless steel is not caused only by strengthening of the α'-martensite phase but also by strengthening of the austenite phase.

Despite the increase in strength, the ductility of the steels was not impaired by the aging treatment. The fracture elongations did not decrease and the stretch-formability measured by Erichsen cup test was even slightly improved in most cases.

The increase in yield strength depends also on the direction of the test. Increasing the degree of cold working increases anisotropy i.e. yield strength values parallel to the rolling direction and transverse to the rolling direction. Ageing, however, affects by reducing this behaviour.

References

[1] R.E. Smallman: “Modern Physical Metallurgy”, Butterworth & Co Ltd, 4th edition, 1985

[2] R.E. Reed-Hill: “Physical Metallurgy Principles”, JPWS Publ. Co, 3rd ed., Boston, 1994

[3] T. Tiainen: “Myötövanheneminen PKK-metalleissa”, Report 21/1978, Tampere University of Technology, 1978

[4] R.W. Rathbun et al. “Strain Ageing Behavior of Austenitic Stainless Steels Containing Strain Induced Martensite”, Scripta mater. 42 (2000), pp. 887-891

[5] S.L. Robinson et al: “Strain-Ageing in Highly Worked 316L Stainless Steel, Practical Feilure Analysis”, Vol. 1(2) April 2001

[6] K.W. Qian and C. Ni: “The Influence of Strain Aging Treatment on the Mechanical Properties of an Austenitic Stainless Steel”, 5th International Congress on Heat Treatment of Materials. Vol. 1, Budapest, Hungary, 20-24 Oct. 1986, pp. 592-599

[7] A.M. Eleiche, C. Albertini and M. Montagnani: “Effects of Strain Rate History on Strain-Ageing Phenomena in AISI 316 Stainless Steel”, Stainless Steels ‘87, Proceedings of the Conference 14-16 September 1987, The Institute of Metals, 1988, pp. 394-404

[8] R. Sandström et al.: “Temperature Dependence of Tensile Properties and Strengthening of Ni Alloyed Austenitic Stainless Steels”, Scand. Journal of Metallurgy 6 (1977) pp. 156-169

[9] J. Talonen, T. Nenonen and H. Hänninen: “Static Strain Ageing of Cold-Worked Austenitic Stainless Steel”, High Ni Steels Congress 2004,Oostende, Belgium, 2004, pp. 113-122

[10] B. Soenen and N. Akdut: “Strengthening of Austenitic Stainless Steels by Static Strain Ageing”, High Nitrogen Steels Congress 2004,Oostende, Belgium, 2004, pp. 141-145

[11] R.L.K. Ruoppa, T.T. Taulavuori: “Influence of Cold Rolling Reduction and Strain Ageing on Forming Properties of Some Austenitic Stainless Steels”, Proceedings of IDDRG 2007 conference, Györ, Hungary, 2007, pp. 579-586

[12] J. Talonen, et al.: “Comparison of different methods for measuring strain induced α’-martensite content in austenitic steels”, Mat. Sc.& Tech., Vol. 20, Dec.2004, pp. 1506-1512

[13] K. Nohara, et al. Y. Ono, N. Ohashi: Strain-Induced Martensitic Transformation in Metastable Austenitic Stainless Steels in Multi-Stage Tensile Deformation at Various Temperatures. Proc. 1. JIM Int. Symp. New Aspects of Martensitic Transformation, Kobe May 10-12 1976, Japan, pp. 315-320.

EFFECTS OF Cu AND Mn ON THE MECHANICAL PROPERTIES AND HOT DUCTILITY OF Cr-Mn AUSTENITIC STAINLESS STEELS

J.S. Lee, Y.D. Lee, Y.Y. Lee

Stainless Steel Research Group, Korea

Abstract

Production of 200 series stainless steels has been increased recently and widely used to substitute for type 304 stainless steels containing nickel, due to big fluctuation of the nickel price. This study was investigated to improve the mechanical properties and hot ductility of Cr-Mn austenitic stainless steels containing 4% Ni for obtaining the same level of yield strength and elongation of type 304 steel. The results of this investigation show that the proper modification of copper and manganese in the chemical composition of Cr-Mn austenitic stainless steels are able to improve the elongation and the hot ductility during hot rolling, thanks to the control of the microstructural stability and grain boundary structure. On the basis of this investigation, a modified Cr-Mn austenitic stainless steel by control of Cu and Mn contents has been developed, which is suitable for the high formable application product.

Introduction

New ferritic and Cr-Mn austenitic stainless steels have been recently developed to replace standard austenitic stainless steel such as 304, for saving the nickel as a raw material cost[1-3]. Production of Cr-Mn austenitic stainless steels containing manganese, copper and nitrogen for saving the nickel has been increased. Cr-Mn austenitic stainless steel containing 4% nickel has been widely used in the application of kitchen utensils and so on. This application requires the stainless steel to have low yield strength and good formability. In fact, the alloy development of Cr-Mn stainless steels deals mainly with a balance between Mn and Cu to get a better uniform elongation, ultimate strength and hot ductility. Therefore, the effect of Cu and Mn on the properties of Cr-Mn austenitic stainless steel containing 4% Ni was investigated to design the optimum alloy composition. For the optimum alloy composition of a high formable stainless steel, the deformation induced martensite content as austenite stability during fabrication should be considered. The application of Cr-Mn austenitic stainless steel partly substituted nickel with copper and manganese has been widely used in a variety of fields, including kitchen utensils such as sink and cooking pans. In this paper, the works on the relationship between mechanical

properties and microstructural changes of these stainless steels are briefly reviewed and therefore, the effect of Cu and Mn on the mechanical properties, formability and hot workability of these stainless steels are investigated and discussed in terms of austenitic stability and hot ductility, varied as the alloy composition.

Experimental

The chemical composition of the stainless steels used in this experiment is shown in Table 1. The stainless steels used were melted and casted into steel mould in the laboratory. The δ-ferrite content of the stainless steel ingots were measured by the ferrite scope instrument. The ingot stainless steels were hot rolled to the plates of 5mm thickness and then cold rolled down to the steel plates of 1 mm thickness. The hot rolled and cold rolled specimens were annealed at 1100°C for 100 seconds, respectively. The mechanical properties and Erichsen formability of the cold rolled stainless steels were measured. The amount of deformation induced martensite during cold rolled reduction was also measured by ferrite scope with the reference of a standard specimen knowing the martensite content. Hot workability of the Cr-Mn austenitic stainless steels with varied content of copper and manganese was measured at the temperature range of 800~1000°C by the Gleeble 3800 tester.

Results and Discussions

Mechanical Properties and Microstructural Stability of Cr-Mn Stainless Steels

Cr-Mn austenitic stainless steel containing low nickel content has been widely used in the application of kitchen utensils, instead of using a type 304 steel. For industrial application it is required to have the properties of low yield strength and high formability. The effects of Cu and Mn on the mechanical properties of Cr-Mn austenitic stainless steel as shown in Table 1 were investigated for replacing the expensive Ni metal.

Table 1. Chemical composition range of the stainless steels used (wt. %)

Steel Grade	C	Si	Mn	Cr	Ni	N	Cu
M-1	0.05	0.50	6.0	16.5	4.3	0.06	0
M-11~M21	0.05	0.50	**5.1~8.0**	16.0	4.0	0.06	**0.7~2.7**

Figure 1 shows the effect of copper on the work hardening rate in the stress-strain curve of the Cr-Mn austenitic stainless steels. The work hardening rates in the curves of the Cr-Mn austenitic stainless steel are decreased with increasing copper content. These curves are crept well at low strain range of 10~20%, but the work hardening rates of the stainless steel containing low copper content are increased at high strain range of 30~40%. The slope of hardening rate of the Cr-Mn austenitic stainless steel, especially without containing copper, is increased rapidly at high strain

rate of 30~40% of the tensile test. This phenomenon can be explained in terms of variation of deformation induced martensite transformation and stacking fault energy by addition of copper during deformation. The amount of deformation induced martensite transformation in the Cr-Mn stainless steels are varied with the microstructure stability depends on their chemical composition.

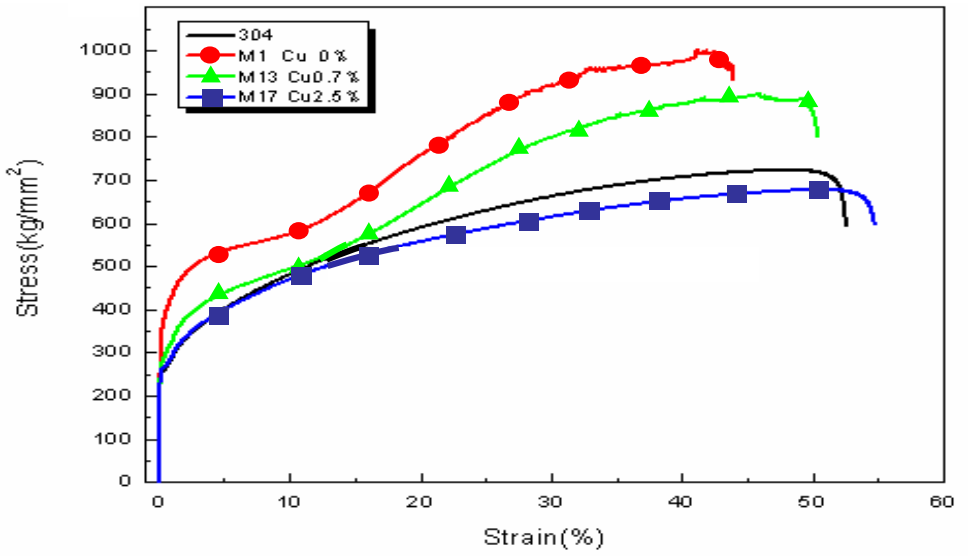

Figure 1. Effect of Cu on the work hardening exponent of the tested stainless steels

Table 2 shows the mechanical properties, deformation induced martensite transformation temperature (Md_{30}) and hot ductility of Cr-Mn austenitic stainless steels varied with copper and manganese. The mechanical properties of these stainless steels depend on their microstructure stability index[4] such as Md_{30} calculated from the chemical composition of the stainless steels as shown in Table 1. Relation between yield strength and elongation of the stainless steels and content of Cu and Mn are analyzed and the regression equations (1) and (2), respectively are obtained as the below.

$$\text{Y.S. (kg/mm}^2\text{)} = 30.4 - 0.92\text{Cu} - 0.22\text{Mn} \quad (\text{R-Sq.} = 66.8\%) \qquad (1)$$

$$\text{El. (\%)} = 15.1 + 21.6\text{Cu} + 6.2\text{Mn} - 2.6\text{Cu}^2 - 1.8\text{CuMn} \quad (\text{R-Sq.} = 72.8\%) \qquad (2)$$

Cu as the most effective element is close related to the yield strength and the elongation, compared to those of Mn element. From the regression analysis equation of elongation the optimum range of Cu and Mn content of the stainless steels for securing lower yield strength and sufficient elongation are 1.7~2.0% and 6.5~7.0%, respectively. The formability of these meta stable austenitic stainless steels is varied with the austenite microstructure stability depends on the elements of Cu, Ni and Mn. Table 2 shows that high Erichsen values as stretch formability are obtained at the stability index of 5~25. The stretch formability of the stainless steels has

relationship between deformation induced martensite transformation during forming and the microstructure stability index as their chemical composition. Table 3 show the δ-ferrite content and Md_{30} temperature of the commercial 200 series stainless steels. The measured δ-ferrite contents from the 200 series austenitic stainless steels means the index of meta stability of microstructure and they are fitted well to that of the calculated by the Sanchez's equation[5].

Table 2. Mechanical properties of the tested stainless steels varied with Cu and Mn

Steel Grade	Cu (%)	Mn (%)	YS (kg/mm^2)	Elongation (%)	Erichsen (mm)	Md_{30} (^oC)	Stability Index	R.A at 900℃ (%)
M1	0	5.95	37.7	43.9	10.94	97	46.7	61.7
M11	1.02	7.55	27.7	53.1	11.21	43	12.6	61.0
M12	2.50	7.54	26.7	52.1	10.78	26	-4.1	54.3
M13	0.72	6.45	28.6	51.1	10.84	87	33.1	62.7
M14	1.77	6.60	26.9	54.3	11.31	55	8.3	62.5
M15	2.70	6.62	26.8	51.6	10.98	30	2.2	52.0
M16	1.00	5.50	28.3	49.8	11.48	86	38.4	62.9
M17	2.56	5.60	26.5	54.3	11.54	46	6.7	57.4
M18	1.78	5.12	27.8	54.6	11.03	70	24.5	50.2
M19	1.77	7.92	26.8	52.8	10.82	48	0.4	53.9
M20	1.77	6.57	27.8	54.6	11.50	59	23.3	58.6
M21	1.75	6.55	26.9	53.5	11.33	59	22.8	60.6

Stability Index=$0.0267x^2+0.4332x-3.146$, *where x=250.4-205.4C-101.4N-7.6Mn -12.1Ni-6.1Cr-13.3Cu*[4]

$Md_{30}(^oC)$=551-462(C+N)-9.2Si-8.1Mn-13.7Cr-29(Ni+Cu)-6.8Nb-1.42(G/SNo.-8.0) [6]

Table 3. Chemical composition of type 202M, 204 and 304 stainless steels (wt. %)

Steel grade	C	N	Cr	Ni	Mn	Cu	Si	Md_{30} (^oC)	Cal. δ-ferrite	δ-ferrite
202M	0.05	0.07	15.7	4.8	7.5	1.10	0.50	44	2.6	2.0
204	0.05	0.18	14.5	1.0	9.9	1.13	0.50	97	2.4	0.9
304	0.05	0.03	18.5	8.1	1.1	0.12	0.50	32*		5.3

* $Md_{30}(^oC)$ =413-462(C+N)-9.2Si-8.1Mn-13.7Cr-9.5Ni-18.5Mo-1.42(G/SNo.-8.0) (Angel's equation)

Calculated δ (%) = 3.6Creq. – 2.75Nieq. – 34.1 (by Sanchez equation [7])

$Cr_{eq.}$ = %Cr+0.7%Si+1.25%Mo+0.055Mn, Ni_{eq}.= %Ni+27.4%C+22.7%N+0.35%Cu

Figure 3 shows the amount of martensite transformation of 200 series stainless steels induced with cold rolled reduction. Based on the equation of Md_{30}[6] temperature, the effect of Cu and Ni on the temperature is minus 29 and it means that the deformation induced martensite transformation is very small. The amount of martensite transformation depends on the microstructure stability and is increased with increasing the cold rolled reduction. The higher

stability index, the more deformation induced martensite transformation is formed. Figure 3 shows the variation of martensite of Cr-Mn stainless steels with cold rolled reduction. The results of the present investigation in Table 2 indicate that the optimum stability index of Cr-Mn stainless steel obtained from a balance between Mn and Cu is around 30. In order to get a better uniform elongation and ultimate strength, the deformation induced martensite temperature and lower yield strength should be considered for an optimization of the chemical composition.

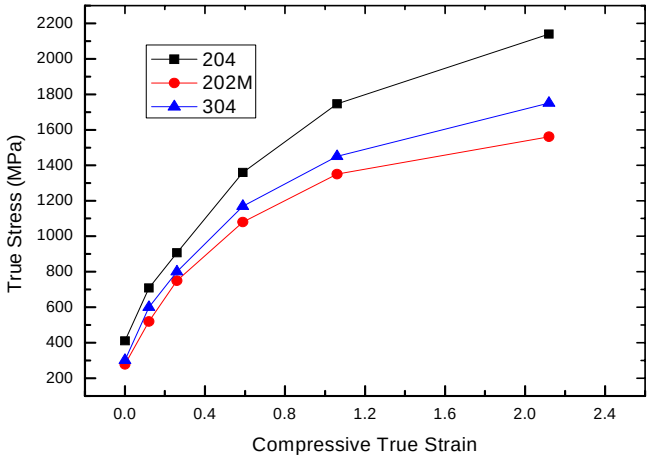

Figure 2. Variation of stress and strain curves with cold rolled reduction of austenitic stainless steels

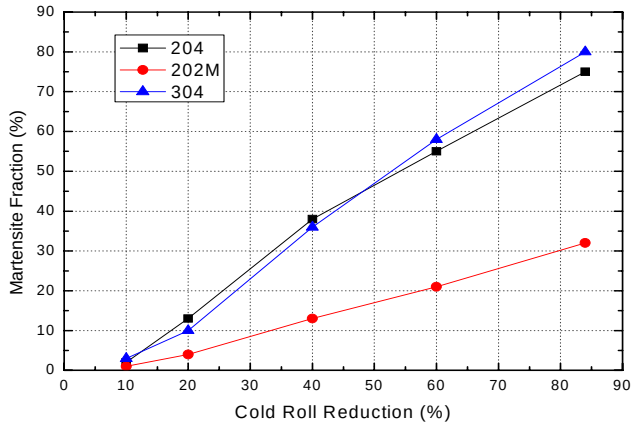

Figure 3. Variation of the martensite induced with cold rolled reduction of different Cr- Mn austenitic stainless steels. (SI 202M =0.4, SI 204=32.0)

Hot Ductility of Cr-Mn Austenitic Stainless Steels

As described in the previous section, copper contributes to decrease the rate of strain hardening and yield strength of the Cr-Mn austenitic stainless steels, as shown in Figure 1. But, it is known that copper deteriorates the hot ductility of the stainless steels, due to the grain boundary segregation[8]. Table 2 shows the reduction area (%) of hot tensile test specimens measured at the temperature of 900°C. The results show that the reduction of area in hot tensile test of Cr-Mn

stainless steels is decreased with increasing copper content.
The decrease of reduction of area in hot tensile test can be explained in terms of liquidation and oxidation of copper at the grain boundary. Based on the results of hot tensile test, the regression equation of Reduction of Area (%) can be obtained as the following equation (3).

$$R.A.(\text{at } 900℃) = -64.29 - 4.56\,Cu + 40.72\,Mn - 3.13\,Mn^2 \quad (R\text{-}Sq. = 62.4\%) \quad (3)$$

As based on the regression equations (2) and (3) for the elongation and hot ductility respectively, the optimum range of Cu and Mn content of the Cr-Mn stainless steels can be calculated. The optimum range of Cu and Mn content for obtaining the elongation of above 54% and the hot reduction area of above 60% at 900°C are around 1.7% and 6.5%, respectively.

Conclusions

The results of the present investigation show that the proper modification of copper and manganese content in the chemical composition of Cr-Mn austenitic stainless steels are able to improve the elongation and the hot ductility during hot rolling, thanks to the control of the microstructural stability and grain boundary segregation. The increase in austenite stabilizing element as copper contributes to strain hardening reduction, which results in low yield strength of Cr-Mn stainless steels. The deformation induced martensite transformation, resulting from the microstructural instability depends on the chemical composition is a major factor for improving the elongation and formability of the austenitic stainless steels. On the basis of this investigation, a modified type 201 austenitic stainless steel by the control of Cu and Mn contents has been developed, which is suitable for the high formable application product and for the good hot workability during hot rolling process.

References

[1] M. Speidel, C. Kowanda and M. Diener, “High Nitrogen Steels” HNS 2003 conference (2003), Institute of Metallurgy ETH Zurich

[2] Y. H. Kim, K.Y. Kim and Y. D. Lee, “Mechanical Properties of Nitrogen Alloyed High Strength Austenitic Stainless Steel for Automotive Application” SAE Conference, Detroit, (2004), “The New Light-Weight Option” SAE International Press p61

[3] J. Charles et al., MDC Project “Chrome-Manganese Stainless Steels” Presentation paper of ISSF-9 Meeting, Helsinki (2005)

[4] US patent No. 6056917 (1998), “Low Nickel Containing Austenitic Stainless Steels”

[5] Y. H. Kim, K. Y. Kim and Y. D. Lee, “Development of High Nitrogen Cr-Mn-Ni Stainless Steels for Automotive Structure” POSCO Technical Reports (2002).

[6] H. Nohara, H. Ono and H. Ohashi, Tetsu-to-Hagane, 63 (1977) 8, p212

[7] T. Oshima, Y. Habara and K. Kuroda, Tetsu-to-Hagane, 93 (2007) 8, p544

[8] C. F. Hull, Proc. American Soc. Test. Mat. 60, (1960) p667

STATIC STRAIN AGEING OF METASTABLE AUSTENITIC STAINLESS STEEL

J. Talonen[1], H. Hänninen[2]

[1]Outokumpu Oyj, Finland, [2]Helsinki University of Technology, Finland

Abstract

Static strain ageing (SSA) of austenitic stainless steel grades EN 1.4318 (AISI 301LN) and EN 1.4301 (AISI 304) was studied. The test materials were pre-strained in tension and subsequently aged at temperatures ranging between 110 and 230°C. Yield strength increases up to 200 MPa due to SSA were observed. The higher was the α'-martensite volume fraction after pre-straining, the higher was the yield strength increase after ageing. However, the maximum strength increase was achieved at α'-martensite volume fraction of about 0.3. Higher α'-martensite volume fractions did not provide further strengthening. Since substantial strengthening was obtained also at low α'-martensite volume fractions, the SSA is believed to involve microstructural changes in the austenite. Possible effects of the SSA on the microstructures of austenite and α'-martensite phases are discussed.

Introduction

Static strain ageing of bcc metals and alloys is a well-known phenomenon and widely exploited in engineering applications. In the bcc metals the SSA involves the formation of atmospheres of interstitial atoms (C and N) around dislocations. Also austenitic stainless steels having fcc crystal structure have been shown to exhibit a substantial increase in the upper yield strength after heat treatments at temperatures around 200°C[1-4]. Although the mechanisms of the SSA of austenitic stainless steels are not yet understood, the phenomenon has been attributed to the presence of strain-induced α'-martensite phase. It has been suggested that the mechanism may involve the re-distribution of interstitial atoms in the strain-induced α'-martensite or the changes in the residual micro-stress state. However, substantial increases in the yield strength may be achieved even at very low α'-martensite volume fractions, indicating that the strengthening is not necessarily related only to the presence of strain-induced α'-martensite phase.

In this paper the SSA of Cr-Ni alloyed austenitic stainless steels was studied. Possible microstructural changes in the austenite phase and the role of the strain-induced α'-martensite phase in the SSA phenomenon were discussed.

Experimental

The experiments were carried out on two austenitic stainless steel grades, EN 1.4318 (AISI 301LN) and EN 1.4301 (AISI 304). The chemical compositions and M_{d30} temperatures[5] of the steels are given in Table 1.

Table 1. Chemical compositions of the test materials

Steel grade	C	Si	Mn	Cr	Ni	Mo	Cu	N	Fe	M_{d30} (°C)
EN 1.4318	0.019	0.48	1.61	17.6	6.6	0.14	0.22	0.094	bal.	37
EN 1.4301	0.041	0.33	1.71	18.2	8.1	0.32	0.37	0.054	bal.	-16

Mechanical testing was carried out with a MTS 810 tensile testing machine. Before the ageing heat treatments the test materials were pre-strained in tension at nominal strain rate of 10^{-3} s^{-1}. Tensile tests after the heat treatments were carried out at $3x10^{-4}$ s^{-1}. The ageing heat treatments shorter than 30 min were performed in oil (temperatures up to 140°C) and in salt bath (temperatures >140°C). Longer heat treatments were performed in a circulating air furnace.

A Ferritescope calibrated with δ-ferrite samples was used to measure the α'-martensite volume fractions. The Ferritescope readings were converted to α'-martensite fractions by multiplying with the factor of 1.7.[6] Some samples were analysed with X-ray diffraction (XRD) before and after ageing heat treatments with equipment comprising Inel MPG goniometer, Inel CPS 120 detector, Siemens Kristalloflex 710H high voltage generator and Co-tube.

Results

Mechanical behaviour

Examples of engineering stress-strain curves of tensile pre-strained EN 1.4318 and EN 1.4301 steels aged at 170°C are shown in Figures 1a and 1b, respectively. The results clearly show that the SSA response was dependent on the pre-strain level and especially on the α'-martensite volume fraction transformed during the pre-straining. In EN 1.4301 steel, in which the α'-martensite volume fraction was only 0.003 after 15 % pre-straining, hardly any effect on the flow curve could be observed. Instead, the EN 1.4318 steel exhibited a well-defined upper yield point and a significant increase in the yield strength after SSA. Furthermore, the yield strength increase became more pronounced with increasing pre-strain and α'-martensite volume fraction. The ductility of the steels was maintained high after the SSA. In fact, the uniform elongation even increased.

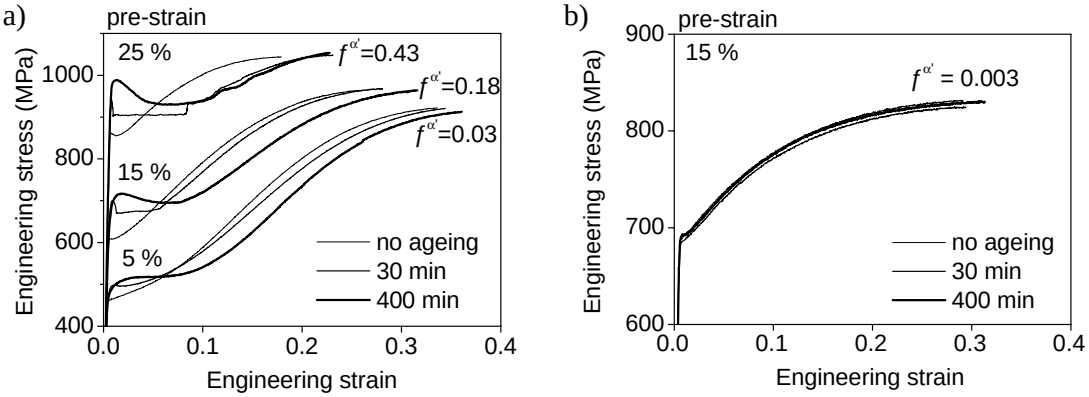

Figure 1. Engineering stress-strain curves of (a) EN 1.4318 steel pre-strained in tension to engineering strains of 5 %, 15 % and 25 % and aged at 170°C and (b) EN 1.4301 steel pre-strained in tension to engineering strain of 15 % and aged at 170°C

The effect of temperature on the SSA response is illustrated in Figure 2, which presents the yield strength increase of 15 % pre-strained EN 1.4318 steel at various temperatures as a function of time. The yield strength increase is defined as the difference between the true stress at the end of pre-straining and the upper yield strength after the SSA. As in any thermally activated process,

the rate of the ageing process increased with increasing ageing temperature. Furthermore, there seemed to exist a temperature-independent maximum level for the yield strength increase. Figure 3 shows that the maximum yield strength increase was clearly dependent on the α'-martensite volume fraction. Furthermore, a given increase in the yield strength was reached much faster at higher pre-strain levels and α'-martensite volume fractions. The higher was the α'-martensite volume fraction after pre-straining, the higher was the maximum yield strength increase. However, the maximum yield strength increase seemed to saturate when the α'-martensite volume fraction exceeded 0.3.

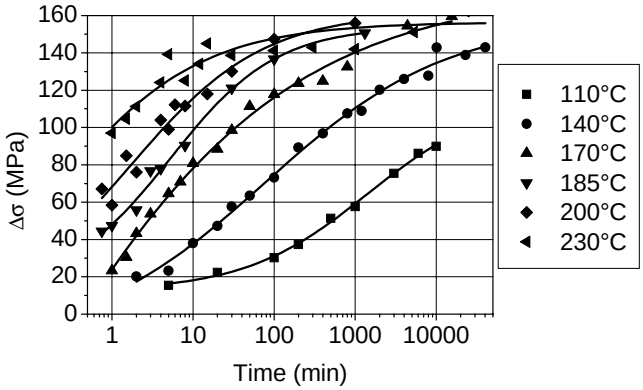

Figure 2. Increase in yield strength of 15 % tensile pre-strained EN 1.4318 steel after SSA at various temperatures as a function of time

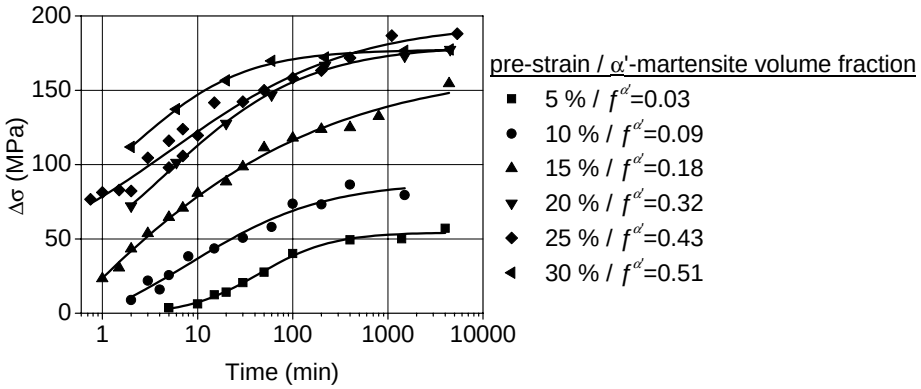

Figure 3. Effect of pre-strain and α'-martensite volume fraction on the yield strength increase due to SSA at 170°C as a function of time

Effect of static strain ageing on microstructure

No change in the α'-martensite volume fraction could be observed after the ageing heat treatments. The XRD measurements indicated small variation of the XRD line shapes. Both austenite and α'-martensite lines became slightly narrower, indicating either rearrangement of dislocations to low-energy dislocation structures or a decreasing dislocation density. However, the changes in the line shapes were overall very small. The most distinct feature of the XRD results was the behaviour of the ε-martensite $10\bar{1}1$ reflection in 15 % pre-strained EN 1.4318 steel. As shown in Figure 4, after ageing at 170°C the reflection was found to disappear gradually. After other pre-strain levels the ε-martensite reflections were not detected.

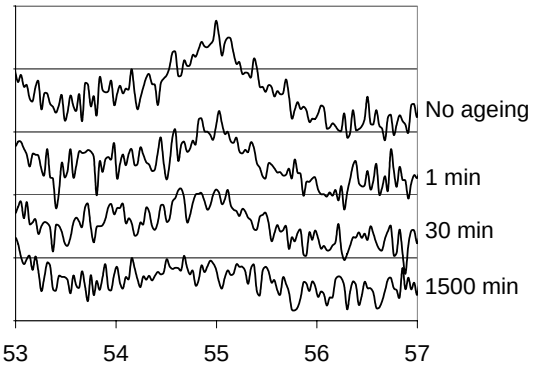

Figure 4. Effect of SSA at 170°C on the intensity of $\varepsilon 10\bar{1}1$ reflection in 15 % pre-strained EN 1.4318 steel

In our earlier study[2], the microstructures of EN 1.4318 steel were examined by TEM before and after ageing at 170°C. According to the results the amount of stacking faults and ε-martensite seemed to decrease, but overall the observed changes were small.

Ageing kinetics

The tensile test results presented in this paper were previously utilised to determine the activation energy of the SSA process[2]. For the 5 %, 15 % and 25 % pre-strained EN 1.4318 steel the activation energies were 130, 134 and 113 kJ/mol, respectively. These values are close to the activation energy of C and N diffusion in austenite[7].

Discussion

Microstructural changes in austenite

Although the degree of strengthening due to SSA was clearly dependent on the α'-martensite volume fraction, at least the following two features indicate that the SSA may be attributed to the microstructural changes in the austenite phase: 1) significant increase in the yield strength was obtained even at very low α'-martensite volume fractions and 2) the activation energy of the SSA process was close to the activation energy of C and N diffusion in austenite. Furthermore, it has been shown[8] that the plastic deformation of an austenite/α'-martensite aggregate is mostly concentrated in the softer austenite phase and the harder α'-martensite does not experience significant plastic deformation, when the α'-martensite volume fraction remains below 0.3. Thus, changes in the mechanical properties of the α'-martensite phase should not cause significant variation in the mechanical properties of the steel, when the α'-martensite volume fraction remains low.

The close relationship between the ageing response and α'-martensite volume fraction is probably caused by the fact that the α'-martensite transformation is triggered by the microstructural changes of the austenite. The sequence leading to the α'-martensite transformation involves the dissociation of perfect dislocations and the associated formation of stacking faults in the austenite. Further generation and overlapping of the stacking faults leads to the formation of bundles of stacking faults, ε-martensite and mechanical twins, collectively referred to as shear bands. The α'-martensite phase then nucleates at the intersections of the shear bands. Thus, the necessary condition for the SSA may not be the presence of α'-martensite phase, but the presence of stacking faults always appearing in conjunction with the α'-martensite phase. Indeed, it has been shown[9] that the deformation microstructures of the EN 1.4318 and

EN 1.4301 steels studied here are very different. While the deformation microstructure of austenite in EN 1.4301 steel consisted mainly of tangled dislocations and some single shear bands, numerous intersecting shear bands dominated the microstructures of EN 1.4318 steel.

The SSA can affect the stacking faults (or shear bands) in two ways: 1) through the temperature dependence of the stacking fault energy (SFE) and 2) by causing the segregation of solute atoms to stacking faults. Since the SFE increases with increasing temperature[10-11], the stacking faults become narrower with increasing temperature. The temperature coefficient of the SFE for the steel compositions and temperatures relevant here is about 0.1 mJ/m^2K[10-11]. Thus, the SFE can be more than doubled during an ageing heat treatment. It is clear that this can significantly alter the deformation microstructure. Increase in the SFE also causes reverse transformation of ε-martensite phase, since it actually forms by overlapping of stacking faults.
In principle, the temperature effect on stacking faults due to the variation of SFE should be reversible. However, the stacking faults and ε-martensite do not reappear to the original extent when the temperature is lowered back to room temperature [11]. This was also observed by the present XRD measurements indicating the disappearance of the ε-martensite reflection. The possible causes of the irreversibility may be, for instance, solute impedance forces, local stress variations or segregation of solute atoms to stacking faults[11]. Enami et al.[12] observed that upon heating of deformed AISI 304 steel the ε-martensite was gradually transformed to irregularly overlapping stacking faults. This is essentially what our present and earlier experiments indicated. While the ε-martensite according to XRD disappeared, TEM still indicated the presence of stacking faults after the ageing[2].

The segregation of the solute atoms to stacking faults, also known as the Suzuki effect[13], may be an important feature causing the SSA. The Suzuki effect is essentially chemical interaction between the interstitial solute atoms and the two atom planes possessing hcp stacking associated to a stacking fault. The hcp phase becomes more stable with increasing solute concentration, which provides the driving force for the segregation. As the hcp phase becomes more stable, the SFE decreases. However, in terms of the SSA phenomenon, probably the most important feature of the Suzuki effect is that an extended dislocation is locked due to the solute atmosphere formation. However, the locking force is only about 1/10 of that of Cottrell effect. Therefore, it seems unlikely that the Suzuki effect alone could account for the observed strengthening effect. Instead, it is probably the combination of the irreversible temperature effects on the stacking faults and the Suzuki effect that account for the yield strength increase associated to the SSA.

Microstructural changes in α'-martensite

Although the microstructural changes in the austenite phase seem to play an important role in the SSA phenomenon, the SSA was clearly dependent on the α'-martensite volume fraction. Figure 5 summarises the effect of α'-martensite volume fraction on the maximum yield strength increase due to the SSA. The data includes the results of the present study as well as previously unpublished results on different austenitic stainless steel alloys pre-strained by both tension and cold rolling.

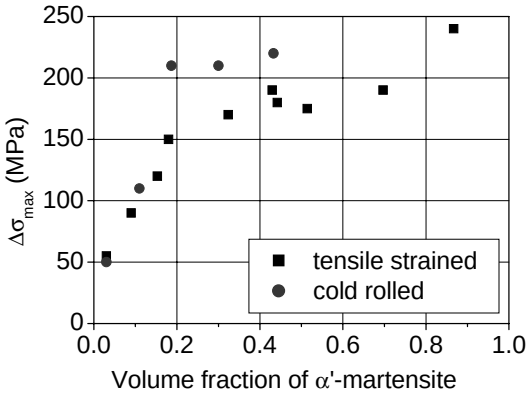

Figure 5. Effect of α'-martensite volume fraction on maximum yield strength increase due to SSA for various austenitic stainless grades pre-strained by tensile straining and cold rolling

The highest yield strength increase seems to be of the order of 200 MPa, and it is reached when the α'-martensite volume fraction is about 0.3. Further increase in the α'-martensite volume fraction does not provide significant additional strengthening. The origin of the behaviour is probably in the percolation of the α'-martensite phase. When the α'-martensite volume fraction exceeds the percolation threshold of 0.3, the plastic deformation of the austenite/α'-martensite aggregate can no longer be fully accommodated by the plastic deformation of austenite[8]. Thus, the α'-martensite starts to contribute to the strength directly by constituting a continuous network throughout the aggregate. Thus, if the SSA is mostly affecting the yield strength of the austenite phase, it does not any longer have as pronounced influence on the behaviour of the aggregate. Of course, any strengthening effects taking place in the α'-martensite should affect the behaviour above the percolation threshold. Since no significant further strengthening above the α'-martensite volume fraction of 0.3 was observed, the SSA probably has only minor effects on the strength of the α'-martensite phase.

Conclusions

Considerable increase in yield strength of metastable austenitic stainless steel may be achieved by means of SSA. Pre-straining and subsequent heat treatment even below 200°C can increase the yield strength more than 200 MPa. The maximum increase in the yield strength seems to be dependent on the amount of strain-induced α'-martensite phase. However, considerable strengthening is achieved even at low α'-martensite volume fractions. Furthermore, the activation energy of the ageing process is close to that of C and N diffusion in austenite. These features indicate that the SSA is related to microstructural changes in the austenite phase, probably involving irreversible temperature effects on stacking faults and Suzuki interaction. Further work is necessary in order to improve the understanding of the mechanisms of the SSA.

References

[1] R.W. Rathbun: "Strain aging behavior of austenitic stainless steels containing strain induced martensite", Scripta materialia, 42, 9, 2000, pp. 887 – 891

[2] J. Talonen, P. Nenonen, H. Hänninen: High Nitrogen Steels 2004, Ostend, Belgium, 2004, p. 113

[3] P. Antoine, B. Soenen, N. Akdut: "Static strain ageing in cold rolled metastable austenitic stainless steels", Materials science forum, 539 – 543, 5, 2007, pp. 4891 – 4896

[4] R.L.K. Ruoppa, T.T. Taulavuori: International deep-drawing research group conference, Györ, Hungary, 2007

[5] K. Nohara, Y. Ono, N. Ohashi: ”Composition and grain-size dependencies of strain-induced martensitic transformation in metastable austenitic stainless steels”, Journal of iron and steel institute of Japan, 63, 5, 1977, pp. 212 – 222

[6] J. Talonen, P. Aspegren, H. Hänninen: ”Comparison of different methods for measuring strain-induced α’-martensite content in austenitic steels”, Materials science and technology, 20, 12, 2005, pp. 1506-1512

[7] R.W.K. Honeycombe, H.K.D.H. Bhadeshia: Steels, microstructure and properties, Edward Arnold, UK, 1995

[8] J. Talonen: Effect of strain-induced α’-martensite transformation on mechanical properties of metastable austenitic stainless steels, doctoral dissertation, Helsinki University of Technology, Finland, 2007

J. Talonen, H. Hänninen: ”Formation of shear bands and strain-induced martensite during plastic deformation of metastable austenitic stainless steel”, Acta materialia, 55, 18, 2007, pp. 6108 – 6118

F. Abrassart: “Stress-induced γ→α’ martensitic transformation in two carbon stainless steels, application to trip steels”, Metallurgical transactions, 4, 9, 1973, pp. 2205 – 2216

R.M. Latanision, A.W. Ruff, jr.: “The temperature dependence of stacking fault energy in Fe-Cr-Ni alloys”, Metallurgical transactions, 2, 2, 1971, pp. 505 – 509

K. Enami, S. Nenno, Y. Minato: “Direct observations of the reverse transformation of ε martensite in type 304 stainless steel”, Transactions of JIM, 18, 5, 1977, pp. 435 – 442

H. Suzuki: Dislocations and mechanical properties of crystals, An international conference held at Lake Placid, John Wiley & Sons, Inc., Lake Placid, USA, 1957, p. 361

THE ROLE OF PRECIPITATION AFTER LONG TIME AGEING IN AN AUSTENITIC STAINLESS STEEL

R. Sandström, L.Z. Jin

Royal Institute of Technology, Sweden

Abstract

During service of high temperature materials, precipitation of different phases can take place. These phases can be expected to significantly influence the mechanical properties of the materials. To quantify these effects the creep resistant austenitic 21Cr 11Ni 2Si 0.2Ni stainless 253 MA has been studied. The steel was exposed to ageing at 700 and 800ºC for up to 5000 h. Precipitation of $M_{23}C_6$-carbides, σ-phase and η-nitrides was observed. The amount of different phases and the particle radii were quantified.
Assuming diffusion controlled growth, the precipitation of the three phases was modelled as a function of temperature. The growth is spherical for σ-phase and essentially planar for the η-nitrides and $M_{23}C_6$. The impingement of the diffusion zones around growing particles is taken into account with a new approach. This impingement is pronounced for the interstitial element nitrogen and its supersaturation limits the final particle sizes. A satisfactory agreement with the metallographic results for particle sizes and their volume fractions was observed.
The precipitation reduces the values for tensile properties elongation, yield strength and tensile strength. Models that explain this behaviour have successfully been established.

Keywords: austenitic stainless, long time ageing, elevated temperature, precipitation, thermodynamic modelling, tensile properties

Introduction

Background

An austenitic stainless steel commonly used for high temperature applications is 253 MA (ASTM UNS S30815). Its composition is 21%Cr 11%Ni 0.17%N with additions of 1.6 wt.% Si and 0.03 wt.% Ce. The silicon and cerium contents give the steel good resistance to oxidation and explains why the steel can be used at such high temperatures as 1100°C in spite of the fact that the steel is not very highly alloyed. The carbon and nitrogen contents are important for its good strength at elevated temperatures [1].

The microstructure continuously changes during high temperature applications and these changes affect the mechanical properties, which can be significantly impaired. For ferritic and martensitic steels the formation of particles during creep and long time ageing has been extensively studied experimentally and modelled. For creep resistant austenitic stainless steels there are few investigations. The same situation applies to the modelling of the precipitation.

The purpose of the present paper is to characterise and model the structural changes in 253 MA during long time ageing and to analyse the influence of the precipitation on the mechanical properties.

Material and microstructure

The composition of the studied heat of 253 MA is given in Table 1. The heat was initially solution heat treated. Part of the material was then long-term aged at 700 and 800ºC for 2000 and 5000 h.

Table 1. Chemical composition of the investigated heat of 253 MA (wt. %)

C	Si	Mn	P	S	Cr	Ni	Mo	Ti	Nb
0.097	1.63	0.55	0.021	<0.001	20.86	10.93	0.32	0.003	0.003
Cu	Co	N	Sn	As	W	V	Al	B	Ce
0.16	0.20	0.191	0.007	0.009	0.030	0.055	0.005	0.0002	0.031

In the solution heat treated condition the material is fully austenitic. No precipitates are present. After ageing at 700 and 800ºC, $M_{23}C_6$-carbides, σ-phase and η-phase are found in this investigation. They form coarse particles after 2000 h. At grain boundaries σ-nitrides and $M_{23}C_6$-carbides are found. They have an elongated shape. Around triple junctions, σ-phase is observed. It is assumed that the particles nucleate at these positions as well. The σ-precipitates are larger than the η-nitrides and $M_{23}C_6$-carbides after long time ageing.

Table 2. Phases found in aged and creep tested 253 MA

Temperature, °C	700	800	900
This investigation, see also [2], [3]	σ+η+$M_{23}C_6$	σ+η+$M_{23}C_6$	
Previous studies [1], [4]-[8]	σ+π+$M_{23}C_6$	σ+π+$M_{23}C_6$	Cr_2N + $M_{23}C_6$

π-phase instead of η-phases was found in previous studies. In the present study no observations were made at 900ºC. The measured average composition of the different phases is given in Table 3.

Table 3. Average compositions of phases observed with EDS in TEM (wt%)

Phase	Formula	Si	Cr	Fe	Ni	Mo	V	N	C
$M_{23}C_6$	$M_{23}C_6$	0.8±0.7	73.6±6.3	13.9±2.3	4.0±3.6	2.8±0.8	0.3±0.2		4.9±4.0
σ	$Cr_{14}Fe_{20}Ni_2Si$	1.7±0.6	38.1±1.9	50.0±3.2	7.2±1.7	0.5±0.4	0.8±0.5	2.2±0.8	-
η	$Cr_3Ni_2SiFe(N)$	8.6±0.8	46.8±1.0	7.9±1.1	31.7±0.7	2.7±0.5	1.2±0.2	2.0±0.3	-

Predictions with Thermo-Calc

The amount of different phases and their composition in thermodynamic equilibrium have been calculated with Thermo-Calc [9]. The Thermo-Calc database TCFE4 has been used. The Cr_2N phase was rejected in the computation, since the phase was not found except near the surface where nitrogen from the air had been penetrating into the material. The phase fractions as a function of temperature are shown in Figure 1.

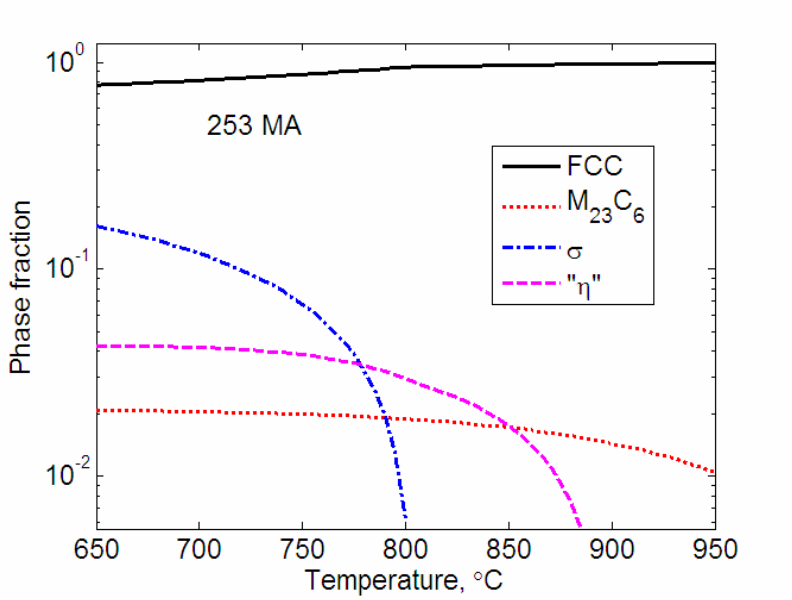

Figure 1. Phase fractions (at.%) as a function of temperature derived with Thermo-Calc

$M_{23}C_6$ is found in the whole temperature range. The amount is between 1 and 2 at.%. σ-phase is formed below 810ºC. The equilibrium content of this phase rapidly increases with decreasing temperature. The η-phase is not directly represented in TCFE4. However, a nitride with the composition Cr_3Fe_2NiN appears in the results. In Table 2, the approximative composition of η is given as $Cr_3Ni_2SiFe(N)$. The composition of the two nitrides is sufficiently close that Cr_3Fe_2NiN can be assumed to represent η, and the analysis in this paper will be based on this assumption. As can be seen in Figure 1, the Cr_3NiN phase appears at temperatures below 900 ºC and its equilibrium content reaches somewhat above 4 % at 650 ºC.
The composition of the observed phases from Thermo-Calc is shown in Table 4. These values should be compared with the measured ones in Table 3.

Table 4. Compositions of phases according to Thermo-Calc at 800 ºC (wt%)

Phase	Si	Cr	Fe	Ni	Mo	Mn	N	C
$M_{23}C_6$	0	72.0	12.8	0.6	9.0	0.1	0	5.4
σ	2.9	39.4	56.8	0.6	0.2	0.1	0	0
η	0.1	48.1	41.1	6.0	0.2	0.1	4.1	0.1

For $M_{23}C_6$ the contents of main elements chromium, iron and carbon are almost the same. For the σ-phase the Cr and Fe values are close. The nickel content is significant in the observation, and surprisingly also nitrogen. For the phase representing η, the chromium contents are close but the observed Ni content is higher than the computed value.

Modelling of precipitation

Nucleation

According to classical theory for nucleation of precipitates the nucleation rate N_r can be expressed as [10], [11]

$$\frac{dN_r}{dt} = \frac{D_{Fe} N_v}{a_0^2} \exp\left(-\frac{G^*}{kT}\right), \quad (1)$$

where D_{Fe} is the self diffusion coefficient, N_v the number of potential nucleation sites at grain boundaries or grain corners per unit volume, a_0 the atomic spacing, G^* the Gibbs energy barrier to nucleation, k Boltzmann's constant and T the temperature in Kelvin. The self diffusion coefficient D_{Fe} and the Gibbs energy barrier G^* can be determined from the thermodynamic and kinetic databases. The Thermo-Calc databases TCFE4 and mob2 have been used.

Growth

Quasi-stationary models based on volume diffusion can be used to describe the velocity for planar and spherical growth [12]. These models can be expressed as

$$\frac{dr}{dt} = \frac{D_{Cr}}{r} \frac{\Omega^2}{2(1-\Omega)} \left(1 - \frac{1}{\Omega_2} \frac{r}{r_{\lim}}\right) \quad \text{(Planar growth)} \quad (2)$$

$$\frac{dr}{dt} = \frac{D_{Cr}}{r} \frac{Z(\Omega)\Omega}{2(Z(\Omega)-1)} \left(1 - \frac{1}{\Omega_2} \frac{r^3}{r_{\lim}{}^3}\right) \quad \text{(Spherical growth)} \quad (3)$$

where

$$Z(\Omega) = \frac{\sqrt{\Omega^2 + 8\Omega} - \Omega}{2\Omega}$$

$$\Omega = \frac{x_{Cr}^{\gamma} - x_{Cr}^{\gamma/\eta}}{x_{Cr}^{\eta/\gamma} - x_{Cr}^{\gamma/\eta}} \quad . \quad (4)$$

and Ω is the non-dimensional supersaturation of the controlling alloying element, in this case chromium. The diffusion of chromium is slower than for iron, nickel, and for the non-metallic elements. x_{Cr}^{γ} is the chromium content of the steel (in at.%) with the matrix γ-phase. $x_{Cr}^{\gamma/\eta}$ is the chromium content of γ in equilibrium with the precipitate in this case η or σ. $x_{Cr}^{\eta/\gamma}$ is the chromium content of the precipitate in equilibrium with γ. r is the thickness of the grain boundary film (planar growth) or radius of the nucleus (spherical growth). D_{Cr} is the diffusion coefficient for chromium. The composition of the matrix and the precipitates was computed with Thermo-Calc.

When a particle grows there is a wake of controlling alloying elements in front of it that is filled with solute from further from the front. However, when the wakes from two particles meet, the stationary situation can no longer be kept and the growth terminates. This is usually referred to as soft impingement. To take this into account, the last factor (in brackets) in Eqs. (2) and (3) has been introduced by modification of the derivation in [12]. Ω_2 is the supersaturation of the element that is first consumed. $r_{\lim}$ in the present case is assumed to be half the grain size when the nucleation occurs at the grain boundaries or corners. When the particle radius r meets the following criterion

$$\left(\frac{r}{r_{\lim}}\right)^n = \Omega_2 \quad (3)$$

the limiting element has been consumed and growth is finished. n = 1 and 3 for planar and spherical growth, respectively

σ-phase

The nucleation of σ-phase takes place at grain corners according to the metallographic observations. Then there is a spherical growth of the precipitates from the corners. This means that Eq. (3) is applicable. One can show that the nucleation is quite fast and can be assumed to occur before the growth. The particle radii versus temperature are given in Figure 2 after different ageing times.

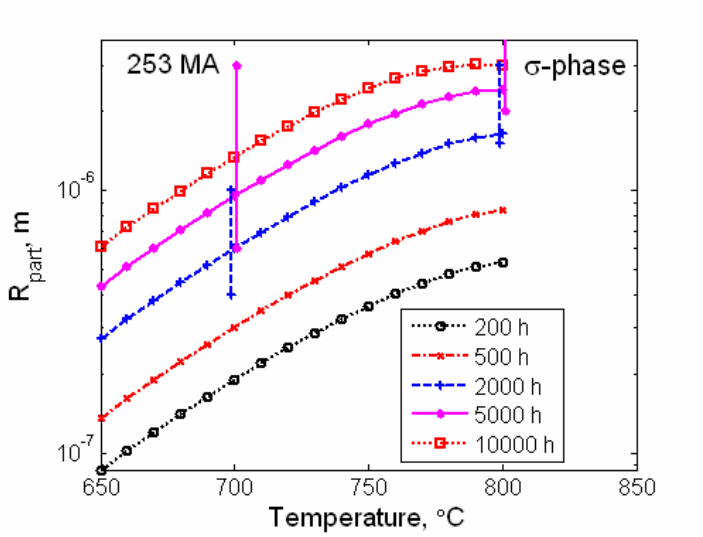

Figure 2. Radii of σ-phase particles as a function of ageing temperatures at different ageing times. Observations are marked with bars.

According to Eq. (3) the growth is parabolic until impingement occurs. Chromium is the limiting element in this case. Since the chromium content is high the effect of the impingement is only seen at the highest temperatures and longest times, where there is a slight drop in the growth rate. In the Figure there is a comparison with experimental data. The agreement between the model and the observations is satisfactory.

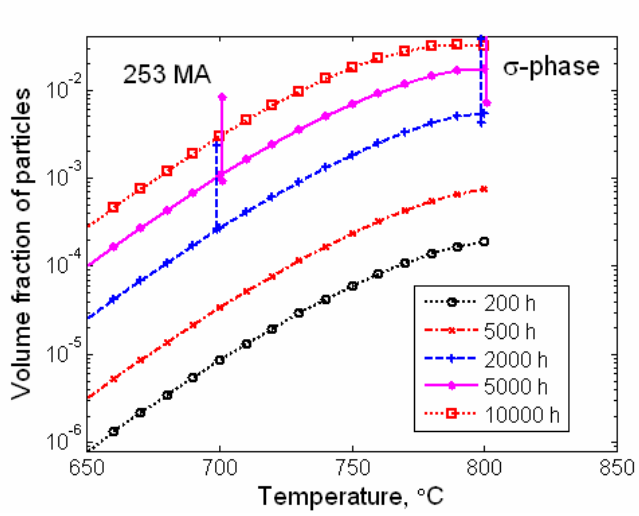

Figure 3. Volume fraction of σ-phase particles as a function of ageing temperatures at different ageing times. Observations are marked with bars.

The volume fraction of σ-phase has been computed using the values in Figure 2 and the assumption that a precipitate is nucleated in each grain corner. The result is shown in Figure 3. The increase in volume fraction with temperature and time is very large. Again there is quite a good agreement with the observations.

η-phase

The η-phase is formed rather homogeneously at the grain boundaries contrary to the σ-phase. The growth is assumed to planar following Eq. (2). The element nitrogen that has the lowest supersaturation for the η-phase, controls the final size of the precipitates. The observations for η both with respect to particle size and volume fraction are well reproduced.

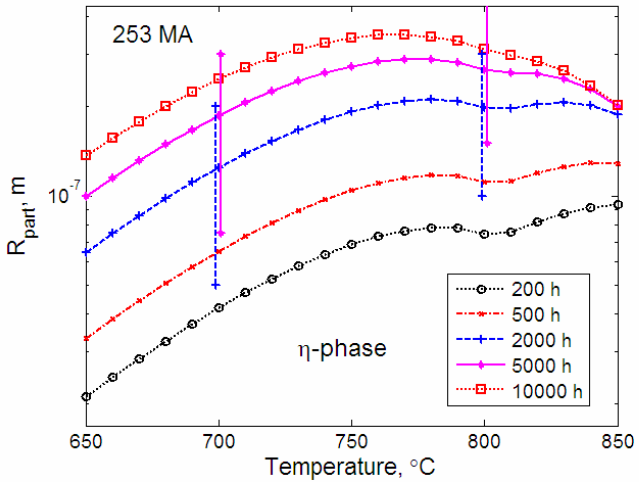

Figure 4. Half width of η-phase particles as a function of ageing temperatures at different ageing times. Observations are marked with bars.

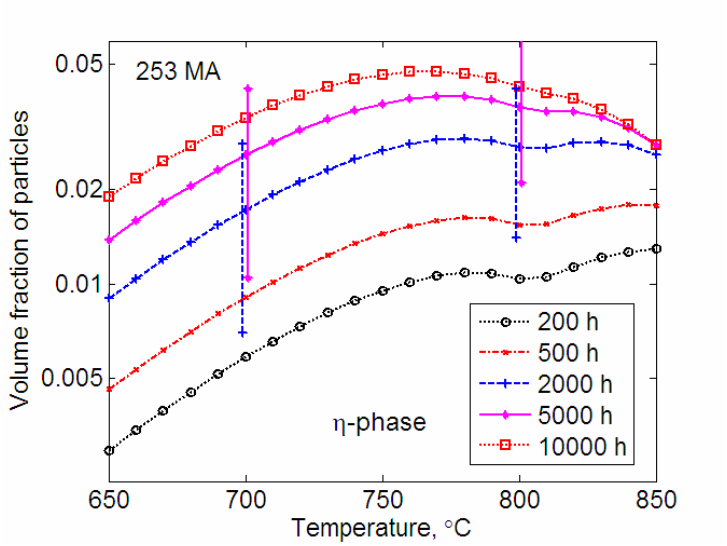

Figure 5. Volume fraction of η-phase particles as a function of ageing temperature at different ageing times. Observations are marked with bars.

Below 750ºC the growth rate increases exponentially with temperature. This is due to the increase in the diffusion coefficient D_{Cr}. In the temperature interval above 750ºC, there is no further increase in the growth rate. This is due to the fact that the further strong increase in D_{Cr} is

compensated by a decrease in the supersaturation Ω. In addition, there is a pronounced effect of soft impingement above 750ºC for the longest annealing times. This can be explained by a decrease in Ω_2 in Eq. (3) with increasing temperature. This variable is given by the following expression, when nitrogen is the limiting element.

$$\Omega_2 = \frac{x_N^{\gamma} - x_N^{\gamma/\eta}}{x_N^{\eta/\gamma} - x_N^{\gamma/\eta}} \quad . \tag{5}$$

$x_N^{\gamma/\eta}$ increases with temperature. Since this variation has a much larger effect in the numerator than in the denominator in Eq. (5), there is a decrease in Ω_2.

$M_{23}C_6$-carbides

The nucleation and growth of the $M_{23}C_6$-carbides occur in a similar way to the η-phase. A parallel growth of the two phases can be observed. Consequently, the carbides nucleate at the grain boundaries and show an essentially planar growth away from the grain boundaries. The half width and the volume fraction of the $M_{23}C_6$-carbides are shown as a function of temperature in Figs. 6 and 7.

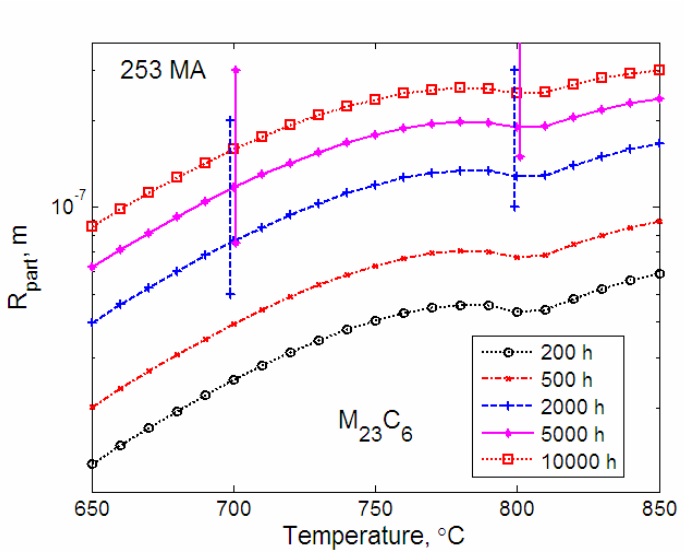

Figure 6. Half width of $M_{23}C_6$-carbides as a function of ageing temperature at different ageing times. Observations are marked with bars.

In the same way as for the η-phase the growth rate increases rapidly up to 750 ºC and then the rate is roughly constant. Ω has about the same temperature dependence for the two phases. The maximum particle width is 0.3 µm. The effect of soft impingement is only marginal. This is at first surprising since Ω_2 is smaller for $M_{23}C_6$ than for the η-phase, for example since the carbon content of the steel is less than that of nitrogen. The reason is that Ω is also smaller for $M_{23}C_6$ than for the η-phase. In fact, $(\Omega)^2$ is about of factor of three smaller for the first phase and the impingement stage has hardly been reached at the longest annealing time.

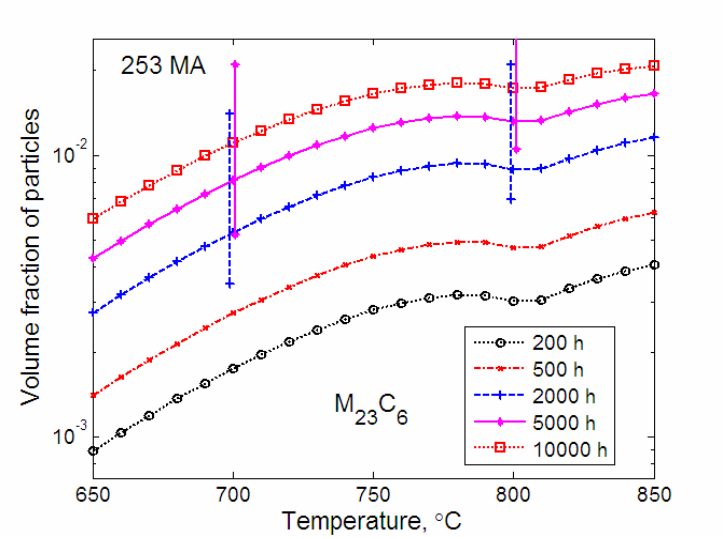

Figure 7. Volume fraction of $M_{23}C_6$-carbides as a function of ageing temperature at different ageing times. Observations are marked with bars.

The maximum volume fraction of $M_{23}C_6$ in Figure 7 is 0.02. This is consistent with the amount of equilibrium phase, see Figure 1. The model is in good agreement with the metallographic observations both in Figs. 6 and 7.

Mechanical properties

Ductility

The limit of the forming capability of a material is controlled by plastic instability. When this instability is reached a crack is rapidly formed and failure occurs. In a tensile test the plastic instability is associated with the uniform elongation and the failure with the total elongation. The stress strain curve for many fcc materials can be described by the Kocks-Mecking relation

$$\sigma = A - Be^{(-\omega\varepsilon)} \tag{6}$$

A, *B* and ω are constants, σ the stress and ε the strain. *A* is approximately the tensile strength and *A*-*B* the yield strength. The instability takes place when the following relation is satisfied

$$\frac{d\sigma}{d\varepsilon} = \sigma \tag{7}$$

This equation thus defines the uniform elongation ε_u and the corresponding stress σ_u. Combining (6) and (7) gives

$$\varepsilon_u = -\frac{\ln\left(\frac{A}{B(\omega+1)}\right)}{\omega} \qquad \sigma_u = A\frac{\omega}{1+\omega} \tag{8}$$

Stress concentrations are present around larger particles. As demonstrated in section 4, the σ-phase forms larger particles than the other phases. The σ-phase particles are located at the corners of cubic grains. The critical position for the plastic instability is between particles at grain edges perpendicular to the loading direction. The stress along such an edge can be expressed as [13]

$$\sigma_{conc} = \sigma_{appl} + \frac{1}{2}\left(1 - \frac{E_{part}}{E_{matr}}\right)\sigma_{appl}\left(\frac{a^2}{r^2} + \frac{3a^4}{r^4}\right) \tag{9}$$

σ_{appl} is the applied stress, and E_{part} and E_{matr} are the elastic modulus in the particle and the matrix respectively. a is the radius of the particles and r is the distance from the centre of a particle. The critical stress level is the average value along an edge

$$\sigma_{ave} = \frac{1}{d_{grain}/2 - a}\int_a^{d_{grain}/2} \sigma_{conc} dr \qquad (10)$$

The stress concentration y_{conc} is given by

$$y_{conc} = \frac{\sigma_{ave}}{\sigma_{appl}}$$

The plastic instability takes place when σ_u divided by the stress concentration y_{conc} is reached

$$\frac{\sigma_u}{y_{conc}} = A - Be^{-\omega\varepsilon_{conc}} \qquad (11)$$

Solving (11) gives the uniform ductility in the presence of the stress concentrations from the particles

$$\varepsilon_{conc} = -\frac{1}{\omega}\ln\left(\frac{A}{B}\left(1 - \frac{\omega}{(\omega+1)y_{conc}}\right)\right)$$

The total elongation ε_{tot} is a factor g larger than the uniform elongation

$$\varepsilon_{tot} = g\varepsilon_{conc} \qquad (12)$$

For 253 MA the following values of the constants have been used

A = 750 MPa, B = 234 MPa, ω = 4, g =2.

In Figure 8, the model values for ductility according to Eq. (12) are plotted against the total volume fraction of particles.

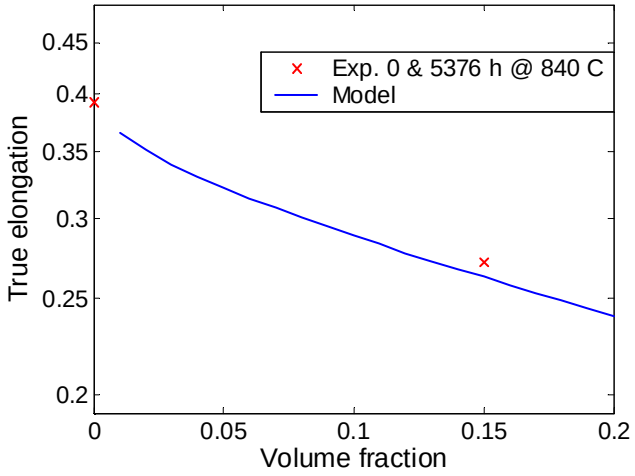

Figure 8. True elongation as a function of the total volume fraction of particles.

A comparison to an experimental point after ageing at 840ºC is given. The important result in Figure 8 is that the true elongation decreases approximately exponentially with increasing volume fraction of particles

$$\varepsilon_{duct} = ae^{-kf_{part}} \qquad (13)$$

f_{part} is the volume fraction of particles, and a and k are constants. k depends on the ratio of the effective elastic modulus in the particles to that in the matrix E_{part}/E_{matr}. This ratio strongly depends on whether cracks are formed around the particles. For 253 MA some cracks appear at these positions and a value of E_{part}/E_{matr} = 0.85 has been assumed. This ratio is hence material dependent.

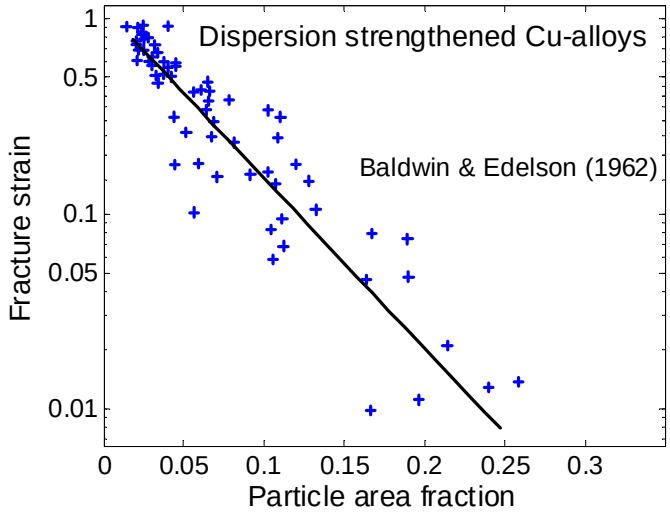

Figure 9. Fracture strain versus strain versus particle fraction for dispersion strengthened Cu-alloys. Experimental from Baldwin and Edelson [14]

In Figure 9, classical results for another fcc material namely dispersion strengthened copper alloys are shown [14]. The results for the ductility follow accurately the behaviour of Eq. (13).

Yield strength

Due to the large size of the particles after ageing, they do not give rise to any strengthening. Thus, there is no particle hardening in 253 MA. However, the precipitates consume alloying elements and this reduces the solid solution hardening. For austenitic stainless steels, solid solution hardening has recently been modelled [15]. In fact, it was found that the hardening could be expressed as

$$\Delta R_{p0.2} = 77\sqrt{N} + 20Mn + 7Cr + 33Si + 2.9Ni + (0.24 + 1.1N)d_{\text{grain}}^{-0.5} \qquad (14)$$

N, *Mn*, *Cr*, *Si*, *Ni* are the element contents in wt.% and d_{grain} the grain size. The composition of the precipitates is given in Table 3. From this table and the computed volume fractions of precipitates the reduction in yield strength $\Delta R_{p0.2}$ can be computed.

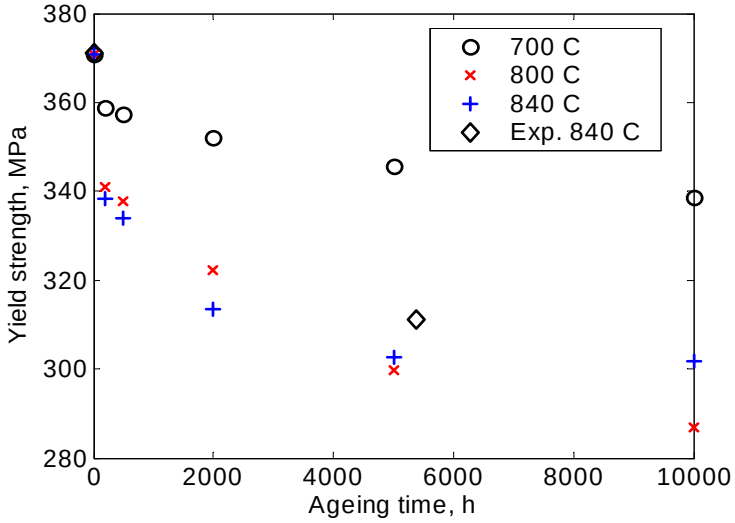

Figure 10. Yield strength as a function of ageing time at 700, 800, and 840ºC. An experimental data point is given at 840ºC.

The results are illustrated in Figure 10. A rapid decrease in the strength is already obtained after a few hundred hours. After that the decrease is slow. The largest decrease is observed at 800ºC. At still higher temperatures the decrease in the yield strength is lower at longer times. This follows from the computed volume fractions in Figs. 3, 5 and 7. The results are consistent with the available experimental data point. No adjustable parameters are involved.

Tensile strength

The tensile strength can be handled in much the same way as the yield strength. Sieurin, Zander and Sandström have generated an expression for the influence of solid solution hardening on the tensile strength R_m. [15]

$$\Delta R_m = 481N + 9.3Cr + 9.5Mo + 13Si - 6.9Ni + 0.21d_{\text{grain}}^{-0.5} \qquad (15)$$

The grain size dependent term is not a function of the composition and does not influence the results in this case and can be ignored. From the composition of the phases in Table 3 and the volume fractions in Figs. 3, 5 and 7, the reduction in tensile strength R_m can be computed.

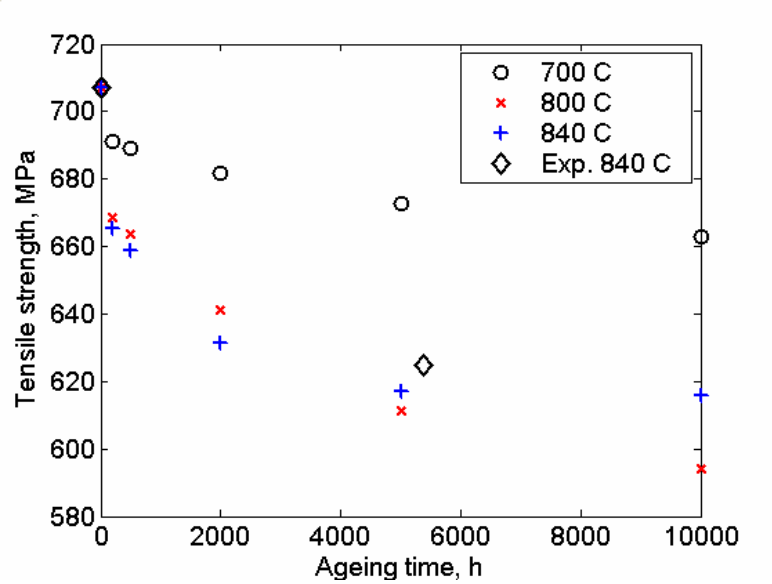

Figure 11. Tensile strength as a function of ageing time at 700, 800, and 840ºC. An experimental data point is given at 840ºC.

The results are shown in Figure 11. In the same way as for the yield strength the decrease is much larger at 800 than at 700ºC. The experimental data point at 840ºC is well represented by the model.

Conclusions

- In the 253 MA grade, σ-phase, $M_{23}C_6$ and η-nitrides are formed after ageing for long times at 700 and 800ºC. In accordance with the metallographic observations, the nucleation of σ takes place at the grain corners followed by a spherical growth. For the η-phase and $M_{23}C_6$ on the other hand the nucleation is homogeneous around the grain boundaries and is followed by planar growth.
- The growth of σ-phase, $M_{23}C_6$ and η-nitrides is controlled by the diffusion of chromium that is slow and for $M_{23}C_6$ and η-nitrides also by the limited access to intermetallic element (soft impingement). The modelled particle sizes and their volume fraction are in good agreement with the observations. A new model has been formulated for the influence of coarse precipitates on the ductility. According to the model, the

ductility decreases exponentially with increasing volume fraction of precipitates. The reduction in yield and tensile strength after long time ageing is modelled as a change in solid solution hardening due to consumption of alloying elements. The model reproduces the experimental data.

Acknowledgements

Financial support from the Consortium for Materials Science in Thermal Energy Processes (KME), Siemens and Outokumpu Stainless is gratefully acknowledged. The authors would like to thank Bo Ivarsson, Outokumpu Stainless for supplying material and data.

References

[1] Yu Maode and R. Sandström, "Influence of Carbon and Nitrogen Content on the Creep Properties of the Austenitic Stainless Steel 253 MA", Scand. J. Metallurgy, 17 (1988) 156-167; Acom, no. 1, pp. 1-13, 1989

[2] H. Liu, "Formation of η-phase in the austenitic stainless steel 253 MA", to be publ. 2008

[3] R. Sandström, L-Z Jin, "Observation and modelling of precipitation during long time ageing in the austenitic stainless steel 253 MA", to be publ. 2008

[4] R. Sandström and Yu Maode, "Factors Controlling the Creep Properties of the Austenitic Stainless Steel 253MA", Creep and Fracture of Engineering Materials and Structures; Swansea UK; 5-10 Apr. 1987. pp. 425-439. 1987

[5] M. Yu, R. Sandström, B. Lehtinen, C. Westman, "Formation of precipitates in the austenite stainless steel 253MA during creep", Scand. J. Metallurgy, 16 (1987) 154-163

[6] Yu Maode and R. Sandström, "Influence of Cerium on the Creep Properties of Austenitic Stainless Steel 253 MA", High Temperature Techn. 6 (1988) 153-157

[7] Yu Maode and R. Sandström, "The Influence of Carbon and Nitrogen on the Creep Characteristics of Avesta 253 MA Steel", Acciaio Inossid., vol. 56, no. 4, pp. 4-16, Oct.-Dec. 1989

[8] G. Selin, Diploma work, "Phase transformations in the heat resistant steel 353 MA, Materials Technology Report KTH/AMT-181", 1998

[9] B. Sundman, B. Jansson, J.-O. Andersson, "The Thermo-Calc Databank System", CALPHAD, vol. 9, no. 2, pp. 153-190, 1985

[10] N. Saunders and A. P. Miodownik, "Evaluation of glass forming ability in binary and ternary metallic alloy systems – an application of thermodynamic phase diagram calculations, Material Science", Materials Science and Technology, 4 (1988) 768-777

[11] J. W. Christian, "The theory of transformations in metals and alloys", third edition, part 1, chapter 10, 2002

[12] G. Engberg, M. Hillert, A. Odén, "Estimation of the rate of diffusion-controlled growth by means of a quasi-stationary model", Scandinavian J. Metallurgy, 4 (1975) 93-96

[13] W.M. Lai, D. Rubin, E. Krempl, "Introduction to continuum mechanics", Butterworth/Heinemann, 1999

[14] W.M. Baldwin and B.I. Edelson, "The effect of second phases on the mechanical properties of alloys", ASM Trans Q. Vol. 55, no. 1, pp. 230-250. Mar., 1962

[15] H. Sieurin, J. Zander, R. Sandström, "Modelling solid solution hardening in stainless steels", Materials Science and Engineering A415, Issues 1-2, 2006, pp. 66-71.

KINETICS OF $\alpha' \rightarrow \gamma$ REVERSION IN A COLD ROLLED AISI 301LN STAINLESS STEEL

S. Rajasekhara[1], P.J. Ferreira[1], P. Karjalainen[2], A. Kyröläinen[3]

[1]The University of Texas at Austin, USA, [2]The University of Oulu, Finland, [3]Outokumpu Stainless Oy, Finland

Abstract

Metastable austenitic stainless steels (SS) transform into martensite (α') upon severe cold rolling. During subsequent annealing the strain-induced martensite reverts to ultra-fine grained austenite (γ). In this context, it is important to develop a fundamental understanding of the kinetics of $\alpha' \rightarrow \gamma$ reversion process. To model the reversion process, we start with the generalized Avrami relationship for diffusion controlled phase transformations, and assume a time and temperature dependent grain growth rate and a time-independent but temperature dependent nucleation rate. On the basis of these assumptions, a generalized model relating volume fraction of reverted austenite with experimental conditions (annealing time and temperature) is derived and the reverted austenite volume fraction calculated. To confirm the validity of this model, a AISI 301LN metastable austenitic SS has been cold rolled to 63% reduction and subsequently annealed at 700°C, 800°C, 900°C and 1000°C for 1, 10 and 100 seconds. The obtained α', γ phase volume fractions are compared with those obtained from the model. A reasonable fit is seen between the experimental data and the model calculation.

Introduction

Currently, there is an increased interest in producing stainless steels with higher mechanical properties [1-2]. A promising approach is to heavily cold roll a metastable austenitic stainless steel to produce deformation induced martensite (α'), followed by a subsequent annealing to produce ultra-fine grained austenite (γ). In this context, it is necessary to understand the phase reversion mechanism to better control the processing variables involved in producing ultra-fine grained austenite. So far, Tomimura *et al.* [3] and Takaki *et al.* [4], have discussed the austenite to martensite transformation in non-commercial SS alloys by analyzing the microstructure evolution. Several other researchers, [5-21], have also described phase changes occurring in cold rolled metastable austenitic SS upon annealing, but the focus of their work was the evaluation of grain sizes and mechanical properties. Therefore, a fundamental understanding of the $\alpha' \rightarrow \gamma$ reversion mechanism is currently lacking. In this context, this work proposes a model to predict the reverted austenite phase fraction as a function of time and temperature. The results from this

model are then compared with the phase fraction data obtained experimentally from heavily cold-rolled and annealed commercial stainless steels.

Model

The volume fraction of a product phase obtained through a diffusion-controlled phase transformation can be calculated as a function of time (t), and temperature (T) according to the generalized form of Avrami's equation, given by [22, 23]:

$$\ln(1-\xi(T,t) = -\left[\frac{4\pi}{3}\right]\int_0^t v^3(T,t)I(T,t)(t-z)^3\,dz,$$

(1)

where $\xi(t,T)$ is the transformed austenite volume fraction, $v(T,t)$ the product-phase grain growth velocity, $I(T,t)$ the nucleation rate and z the incubation time for the formation of the first product-phase nuclei. In order to solve equation (1), we first need to calculate the grain growth velocity - $v(T,t)$. The grain growth velocity can be obtained from differentiating the generalized grain growth law, which is expressed by [24-31]:

$$\left(\bar{\mathbf{d}} - \bar{\mathbf{d}}_\mathbf{o}\right)^n = kt,$$

(2)

where $\bar{\mathbf{d}}$ is the average grain of the product phase, $\bar{\mathbf{d}}_\mathbf{o}$ the initial grain size of the product phase, n the grain growth exponent, k the grain growth parameter and t the annealing time. Hence, the grain growth velocity can be given as:

$$v(T,t) = \frac{\partial \bar{\mathbf{d}}}{\partial t} = \frac{\partial}{\partial t}\left(\bar{\mathbf{d}}_\mathbf{o} + (kt)^{\frac{1}{n}}\right) = \frac{(kt)^{\frac{1}{n}}}{nt},$$

(3)

where all the symbols have the same meaning as before. Assuming a constant nucleation rate for a given annealing temperature, $I(T,t)$ can be expressed as [32-34]:

$$I(T,t) = \omega C_1 \exp\left(-\frac{\Delta G_{diff}}{k_B T}\right)\exp\left(-\frac{\Delta G_{het}}{k_B T}\right),$$

(4)

where ω is the Debye frequency, C_1 the concentration of austenite nuclei, ΔG_{diff} the activation energy for diffusion of solute atoms in the austenite phase and ΔG_{het} the activation energy for product phase nucleation at heterogeneous nucleation sites, such as grain boundaries. Combining equations (1), (3) and (4), equation (1) can be rewritten as:

$$\ln(1-\xi(T,t) = -\left[\frac{4\pi\omega C_1}{3}\right]\exp\left(-\frac{\Delta G_{diff}}{k_B T}\right)\exp\left(-\frac{\Delta G_{het}}{k_B T}\right)\int_0^t\left(\frac{(kt)^{\frac{1}{n}}}{nt}\right)^3 (t-z)^3\,dz,$$

(5)

for which the solution is shown in equation (6):

$$\xi(t,T) = 1-\exp\left(-\left[\frac{4\pi\omega C_1 k^{\frac{3}{n}} t^{\frac{3}{n}+4}}{3n^3}\right]\exp\left(-\frac{\Delta G_{diff}+\Delta G_{het}}{k_B T}\right)\right),$$

(6)

Calculation of nucleation rate – $I(T,t)$

According to equation (46), $I(T,t)$ depends on the concentration of nucleation sites C_1, the change in Gibbs free energy for heterogeneous nucleation ΔG_{het} and the activation energy for atomic diffusion ΔG_{diff}. In turn, the concentration of nucleation sites depends on type of defects considered. In this model, we assume the nucleation to occur at martensite grain boundaries. In this case, C_1^{gb} can be estimated as $C_1^{gb} = C_0\delta_{gb}$, where C_0 is the equilibrium concentration of nucleation sites available if austenite nucleation occurs in the bulk [33], which can be calculated from the molar volume of SS as $C_0 \sim 8.76\times10^{28}\,\mathrm{m}^{-3}$, and the term $\delta_{gb} = \frac{\mathbf{d_{gb}}}{\bar{\mathbf{d}}_\mathbf{o}}$, where $\mathbf{d_{gb}}$ is the grain boundary width ~ (0.5nm) and $\bar{\mathbf{d}}_\mathbf{o}$ the initial austenitic grain size ~ 0.1μm, obtained from experimental observations [35]. The next step is to estimate the activation energy for heterogeneous nucleation ΔG_{het}, which can be expressed as $\Delta G_{het}^{gb} = S(\theta)\Delta G_{\mathrm{hom}}$, where ΔG_{hom} is the change in Gibbs free energy for homogeneous nucleation and $S(\theta)$ is a shape factor due to the presence of grain boundaries [33]. Both of these parameters can be calculated by applying the classical theory of nucleation as discussed by various researchers [32-34].

Activation energy for diffusion

To determine the activation energy for diffusion ΔG_{diff} during the $\alpha' \rightarrow \gamma$ reversion, the elements Ni, Cr and N were considered due to their important role in stabilizing the austenite phase and their concentration in the alloy. The activation energy values for these elements in the bcc and

fcc phases were obtained from the literature [38]. As expected, the substitutional elements Cr and Ni have comparable diffusion activation energies in both phases (Cr: 2.47 eV/mol in bcc and 2.6 eV/mol in fcc, whereas Ni: 2.48 eV/mol in bcc and 2.82 eV/mol in fcc), whereas the diffusion activation energy for nitrogen is twice as large in the fcc phase (1.75 eV/mol) than in the bcc phase (0.82 eV/mol).

Results and Discussion

The parameters needed to run the aforementioned model, namely n and k, C_1, ΔG_{diff} and ΔG_{het} were determined for a AISI 301LN stainless steel (Table 1), which was heavy cold-rolled (63%) at room temperature to produce martensite and subsequently annealed at 700°C, 800°C, 900°C and 1000°C for 1, 10 and 100 seconds, to produce nano/sub-micron austenite grains [35].

Table 1. Chemical composition (in wt %) of AISI 301LN SS used in this work.

	C	N	Ni	Cr	Mn	Si	Cu	Mo
301LN	0.017	0.15	6.5	17.3	1.29	0.52	0.2	0.15

Calculation of $\xi(T,t)$ - Austenite nucleation at the grain boundaries

As Cr and Ni have the highest activation energies for diffusion, it is assumed that these solute atoms are the rate-limiting factor in the $\alpha' \rightarrow \gamma$ phase reversion and thereby will control the reversion kinetics. On this basis, equation (6) can be modified in the form:

$$\xi_{gb}^{chromium}(t,T) = 1 - \exp\left(-\left[\frac{4\pi\omega C_1 k^{\frac{3}{n}} t^{\frac{3}{n}+4}}{3n^3} \right] \exp\left(-\frac{\Delta G_{diffusion}^{chromium} + S(\theta)\Delta G_{\text{hom}}}{k_B T} \right) \right)$$

(7a)

$$\xi_{gb}^{nickel}(t,T) = 1 - \exp\left(-\left[\frac{4\pi\omega C_1 k^{\frac{3}{n}} t^{\frac{3}{n}+4}}{3n^3} \right] \exp\left(-\frac{\Delta G_{diffusion}^{nickel} + S(\theta)\Delta G_{\text{hom}}}{k_B T} \right) \right)$$

(7b)

Calculated values of $\xi(t,T)$ obtained from equations (7a) and (7b) are shown in Figure 1. Two observations can be made. The first is that the phase reversion is quite sensitive to the activation energies for diffusion – as seen in Figure 1a and Figure 1b. A difference of ~ 20kJ/mol between the activation energies for diffusion of Cr and Ni results in substantially different phase fractions. The second observation is that the phase reversion model based on Cr diffusion gives an estimate

of austenite phase fraction (at an annealing temperature of 700°C and 1 second of annealing duration), which is quite close to what is experimentally observed.

A phase reversion model solely driven by nitrogen diffusion was also considered. However, the results indicated that for the abovementioned annealing parameters, the $\alpha' \rightarrow \gamma$ reversion is complete only after 100 seconds. Thus, as expected, substitutional solute atoms seem to be controlling the reversion kinetics. In the future, the model developed herein may be further improved by considering: (1) the volume loss due to secondary phase precipitation, (2) the Cr loss that has diffused to the precipitates, and (3) austenite nucleation on dislocations.

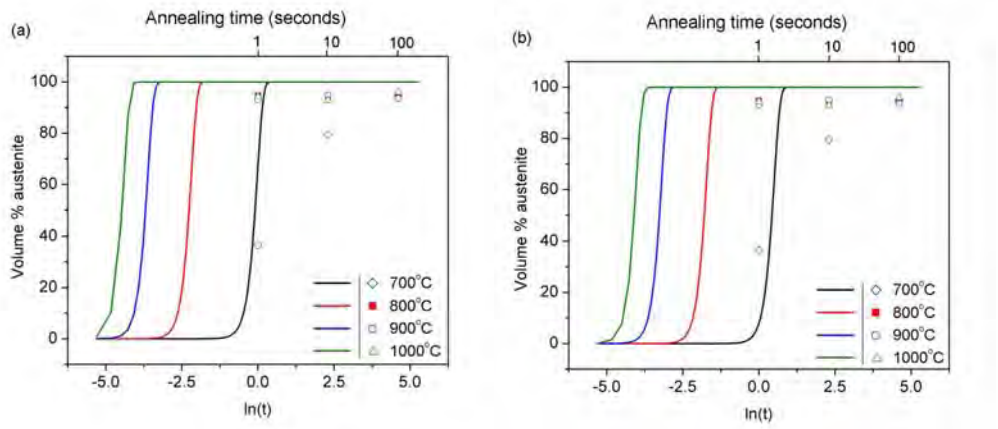

Figure 1. Volume % of austenite during the $\alpha' \rightarrow \gamma$ reversion, assuming (a) Cr-diffusion controlled and (b) Ni-diffusion controlled. The lines are calculated from the model.

Conclusions

The key contributions of this work are as follows:

- The generalized model for the martensite-austenite phase transformation proposed here can be used to predict the austenite phase fraction as a function of time and temperature.
- From first principles kinetics, the proposed model shows that the martensite $\rightarrow$ austenite phase transformation in AISI 301LN SS is diffusion controlled.
- The model proposes that the phase transformation from martensite to austenite is diffusion-controlled by substitutional atoms, in particular, chromium.

References

[1] European steel technology platform, Strategic research agenda; A vision for the future of the steel sector', *European Commission, Belgium*, December 2005

[2] Steel grades, properties and global standards, Outokumpu Stainless Oy.

[3] K. Tomimura, S. Takaki, Tokunaga, Y., *ISIJ International* 31 (1991): 1431-1437

[4] S. Takaki, K. Tomimura, S. Ueda, *ISIJ International* 34 (1994): 522-527

[5] K. Tomimura, S. Takaki, S. Tanimoto, Y. Tokunaga, *ISIJ International* 31 (1991): 721-727

[6] Y. –K. Lee, H. –C. Shi, D. –S. Leem, J. –Y. Choi, W. Jin, C. –S. Choi, *Mater. Sci. Tech.*, 19 (2003): 393-398

[7] M. C. Somani, L. P. Karjalainen, M. Koljonen, P. Aspegren, T. Taulavuori, A. Kyröläinen, *Proc. 5th European Cong., Stainless Steel Science and Markets, Seville,* Sept. (2005): 37-42
[8] M. C. Somani, L. P. Karjalainen, A. Kyröläinen,, T. Taulavuori, *Mater. Sci. Forum* 539-543 (2007): 4875-4880
[9] M. C. Somani, L. P. Karjalainen, P. Juntunen, S. Rajasekhara, P. J. Ferreira, A. Kyröläinen, *International Symposium on Ultra-fine Grained Steels, September 2005, Sanya, China*
[10] P. Juntunen, M. C. Somani, L. P. Karjalainen, A. Kyröläinen, *International Symposium on Advanced Steels, April 2007, Chennai, India*
[11] A. di Schino, I. Salvatori, J. M. Kenny, *J. Mater. Sci.* 37 (2002): 4561-4565
[12] A. di Schino, M. Barteri, J. M. Kenny, *J. Mater. Sci. Lett.*, 21 (2002): 751-753
[13] A. di Schino, M. Barteri, J. M. Kenny, *J. Mater. Sci.*, 38 (2003): 4725- 4733
[14] A. di Schino, J. M. Kenny, M. G. Mecozzi, M. Barteri, *J. Mater. Sci.*, 35 (2000): 4803-4808
[15] J. F. Breedis, *Trans. Am. Inst. Metall. Engg.*, 236 (1966): 218-219
H. Kessler, W. Pitsch, *Acta Metall.*, 15 (1967): 401-405
[16] S. Jana, C. M. Wayman, *Trans. Am. Inst. Metall. Engg.*, 239 (1967): 1187-1193
[17] H. Smith, D. R. F. West, *J. Mater. Sci.*, 8 (1973): 1413-1420
[18] K. B. Guy, E. P. Butler, D. R. F. West, *Met. Sci.*, 17(1983): 167-176
[19] P. M. Kelly, J. Nuttig, *J. Iron Steel Inst.*, March (1961): 199-211
[20] Y. Ma, J. –E. Jin, Y. –K. Lee, *Scripta Mater.,* 52 (2005): 1311-1315
[21] V. Erukhimovitch, J. Baram, *Phys. Rev. B*, 50 (1994): 5854-5856
[22] V. Erukhimovitch, J. Baram, *Phys. Rev.* B, 51 (1995): 6221-6230
[23] G. Gottstein, L. S. Shvindlerman, *Grain Boundary Migration in Metals*, 1st Ed., Boca Raton, CRC Press (1999)
[24] P. Feltham, *Acta Metall.*, 5 (1957): 97-105
[25] M. Hillert, *Acta Metall.*13 (1965): 227
[26] G. T. Higgins, *Met. Sci.*, 9 (1974): 143-150
[27] N. P. Louat, *Acta Metall.*, 22 (1974): 721-724
[28] H. Hu, B. B. Rath, *Metall. Trans.*, 1A (1970): 3182-3184
[29] H. V. Atkinson, *Acta Metall.*, 36 (1988): 469-491
[30] H. Fredriksson, *Mater. Sci. Tech.*, 6 (1990): 811-817
[31] J. W. Christian, '*The Theory of Transformations in Metals and Alloys – An Advanced Textbook in Physical Metallurgy'*, 2nd Ed. London, Oxford Press (1975)
[32] D. A. Porter, K. E. Easterling, *Phase Transformations in Metals and Alloys*, 1st Ed. London, Chapman & Hall (1990)
[33] F. J. Humphreys, M. Hatherly, *Recrystallization and related annealing phenomena*, 2nd Ed. Boston, Elsevier (2004)
[34] S. Rajasekhara, Ph. D. Dissertation, *Development of nano/Sub-micron grain structures in metastable austenitic stainless steels*, The University of Texas at Austin, (2007)
[35] J. Miettinen, *Metall. Trans.*, 28B (1997): 281-297